AGU PUBLICATIONS

JGR

Journal of Geophysical Research: Solid Earth

RESEARCH ARTICLE

10.1002/2017JB014049

Key Points:
- Shear strength following normal stress change depends on slip independent of the sense of normal stress change
- Slip rate depends on normal stress change, friction, and stiffness

Correspondence to:
N. M. Beeler,
nbeeler@usgs.gov

Citation:
Kilgore, B., N. M. Beeler, J. Lozos, and D. Oglesby (2017), Rock friction under variable normal stress, *J. Geophys. Res. Solid Earth*, *122*, doi:10.1002/2017JB014049.

Received 10 FEB 2017
Accepted 20 JUN 2017
Accepted article online 21 JUN 2017

©2017. American Geophysical Union. All Rights Reserved.

Rock friction under variable normal stress

Brian Kilgore[1], N. M. Beeler[2], Julian Lozos[3], and David Oglesby[4]

[1]U.S. Geological Survey, Menlo Park, California, USA, [2]U.S. Geological Survey, Vancouver, Washington, USA, [3]Department of Geological Science, California State University, Northridge, Northridge, California, USA, [4]Department of Earth Sciences, University of California, Riverside, California, USA

Abstract This study is to determine the detailed response of shear strength and other fault properties to changes in normal stress at room temperature using dry initially bare rock surfaces of granite at normal stresses between 5 and 7 MPa. Rapid normal stress changes result in gradual, approximately exponential changes in shear resistance with fault slip. The characteristic length of the exponential change is similar for both increases and decreases in normal stress. In contrast, changes in fault normal displacement and the amplitude of small high-frequency elastic waves transmitted across the surface follow a two stage response consisting of a large immediate and a smaller gradual response with slip. The characteristic slip distance of the small gradual response is significantly smaller than that of shear resistance. The stability of sliding in response to large step decreases in normal stress is well predicted using the shear resistance slip length observed in step increases. Analysis of the shear resistance and slip-time histories suggest nearly immediate changes in strength occur in response to rapid changes in normal stress; these are manifested as an immediate change in slip speed. These changes in slip speed can be qualitatively accounted for using a rate-independent strength model. Collectively, the observations and model show that acceleration or deceleration in response to normal stress change depends on the size of the change, the frictional characteristics of the fault surface, and the elastic properties of the loading system.

1. Introduction

A long-held, simplifying assumption in seismology is that fault slip produces no change in on-fault normal stress [e.g., *Richards*, 1976; *Hardebeck and Hauksson*, 2001]; this idea derives from simple fault models such as a vertical, planar strike-slip fault in an elastically homogeneous material. While this idea has many merits, all known natural faults have some degree of geometrical complexity and are embedded in heterogeneous or anisotropic material surroundings with depth-varying ambient stresses and material properties. Accordingly, fault slip induces some change in on-fault normal stress and potentially makes fault strength during rupture propagation and arrest more spatially variable and time dependent than it otherwise would be [e.g., *Harris et al.*, 1991; *Andrews and Ben-Zion*, 1997; *Bouchon and Streiff*, 1997; *Harris and Day*, 1997]. Most often an Amontons friction assumption, shear resistance proportional to normal stress, is used to characterize friction in simulations, and the effects of slip-induced changing normal stress are particularly expected near bends and stepovers along the fault surface. Normal stress change may either clamp or unclamp a fault, depending on the geometry, which makes the affected fault segment less or more favorable to rupture, respectively, as shown in dynamic models [*Harris and Day*, 1993; *Kame et al.*, 2003; *Bhat et al.*, 2004; *Duan and Oglesby*, 2005; *Oglesby*, 2005; *Lozos et al.*, 2011]. These models of propagation through stepovers in an otherwise homogeneous, isotropic half-space are consistent with *Wesnousky*'s [2006] analysis of historical surface rupture traces, finding that two thirds of surface rupturing earthquakes terminate at geometrical complexities in the previously mapped fault trace, while the remaining third indicate that rupture propagates through complexity under some circumstances. In addition to geometrical complexity, there are instances where material or stress heterogeneity is important in inducing normal stress change. Two common circumstances are faults along a bimaterial interface that are dynamically clamped or unclamped during rupture, which might lead to rupture directivity under particular circumstances [*Andrews and Ben-Zion*, 1997; *Harris and Day*, 2005], and dip-slip faults where dynamic normal stress changes are associated with propagation to the Earth's surface. Generally, a detailed understanding of how shear resistance responds to changes in normal stress is key in predicting near-fault ground motion and evaluating whether or not rupture can propagate through particular zones of material and geometrical complexity.

Normal stress change is also important in earthquake triggering. Stress transfer from seismic and aseismic fault slip to other faults in the surrounding region influences the occurrence of earthquakes; such triggered seismicity makes up a significant fraction of earthquake catalogs. Near-field and far-field aftershocks are the most commonly cited evidence for stress triggering though whether aftershocks are induced predominantly in the near field by static or dynamic stress changes is debated [*Felzer and Brodsky*, 2006; *Richards-Dinger et al.*, 2010]. Evidence of very far field triggering by dynamic stresses is relatively rare but nonetheless well documented [*Hill*, 2012]. Foreshock-main shock pairs also are widely thought to be related through stress transfer. Implicit in stress triggering are fault normal stress changes, though these are mostly treated very approximately, even significantly discounted in static stress triggering studies through choice of a low effective friction coefficient [e.g., *Stein*, 1999]. Only recently have laboratory-based representations of the response of faults to normal stress change been incorporated into stress triggering and earthquake seismicity rate calculations [*Dieterich*, 2007; *Fang et al.*, 2011].

Unfortunately, experimental studies of how fault strength responds to changes in normal stress are not in uniform agreement. The early studies were on bare rock surfaces [*Hobbs and Brady*, 1985; *Olsson*, 1988; *Linker and Dieterich*, 1992]. All of these tests at room temperature involved rapid changes in normal stress imposed on a fault slipping initially at a constant rate. While the results are not identical, they all conclude that the frictional response to a step change in normal stress is a multistage process. *Hobbs and Brady*'s [1985] experiments on gabbro produced a response curve that included a large instantaneous shear stress response, followed by an exponential time-dependent evolution to steady state. *Olsson* [1988] tests on welded tuff produced an immediate steep linear response, followed by a time- or slip-dependent exponential evolution.

Linker and Dieterich [1992] is the most detailed of these studies. Their experiments on Westerly granite using a double direct shear apparatus (DDS) showed a three-stage shear stress response following a normal stress increase (Figure 1a). The first stage is an instantaneous increase in shear stress; this is a machine effect in which shear stress changes with normal stress due to elastic strain of the samples or slight misalignment of the sample and loading frames. This is followed by an immediate increase in shear stress that is linear in time or load point displacement. Linker and Dieterich's interpretation is that in this stage the sudden increase in normal stress increases the contact area on the fault surface, which causes an immediate increase in the fault strength. As a result, the fault's slip rate immediately decreases and the measured shear stress rises linearly with time as load point displacement rate exceeds the fault slip rate, such that the linear slope is the product of the testing machine stiffness and the loading rate. This second stage is the largest part of the fault response. The final stage is a gradual, approximately exponential in load point displacement, increase in shear stress toward a steady state value. Following *Linker and Dieterich* [1992] nearly exactly in experimental approach, *Hong and Marone* [2005] conducted experiments on quartz gouge rather than bare rock surfaces. They also found a three-stage frictional response, though their published data have been corrected for the machine response stage (Figure 1b). Their interpretation is identical to *Linker and Dieterich*'s [1992], and they also find that the immediate shear stress increase is a larger part of the overall frictional response than the gradual exponential evolution to steady state.

Linker and Dieterich [1992] developed constitutive relations that are intended to describe the empirically observed two-stage response of the fault to changes in normal stress. These relations have been used to determine the stability of slip on inclined faults in which shear stress and normal stress are coupled [*Dieterich and Linker*, 1992] and in stress triggering studies [*Dieterich*, 2007; *Fang et al.*, 2011]. It is important to note, however, that these relations cannot be easily applied without modification in dimensioned simulations of dynamic rupture, particularly in the case of slip between elastically dissimilar materials [*Rice et al.*, 2001; *Ranjith and Rice*, 2001]. Rice and coworkers found *Linker and Dieterich*'s [1992] and all constitutive equations that allow an immediate change in shear resistance accompanying a normal stress change to be unstable and to have no solution. If, instead, shear resistance evolves with time or displacement following a change in normal stress, solutions can be obtained (see the original study for more details). To represent the effects of normal stress changes on shear resistance, Rice and coworkers used an alternative relation of *Prakash* [1998] that was based on experimental observations from shock loading experiments on engineering materials, rather than rock.

Prakash [1998] conducted plate-impact experiments; this type of test inherently eliminates testing machine response. *Prakash* [1998] inferred the shear stress on a sliding interface and found that it does not respond

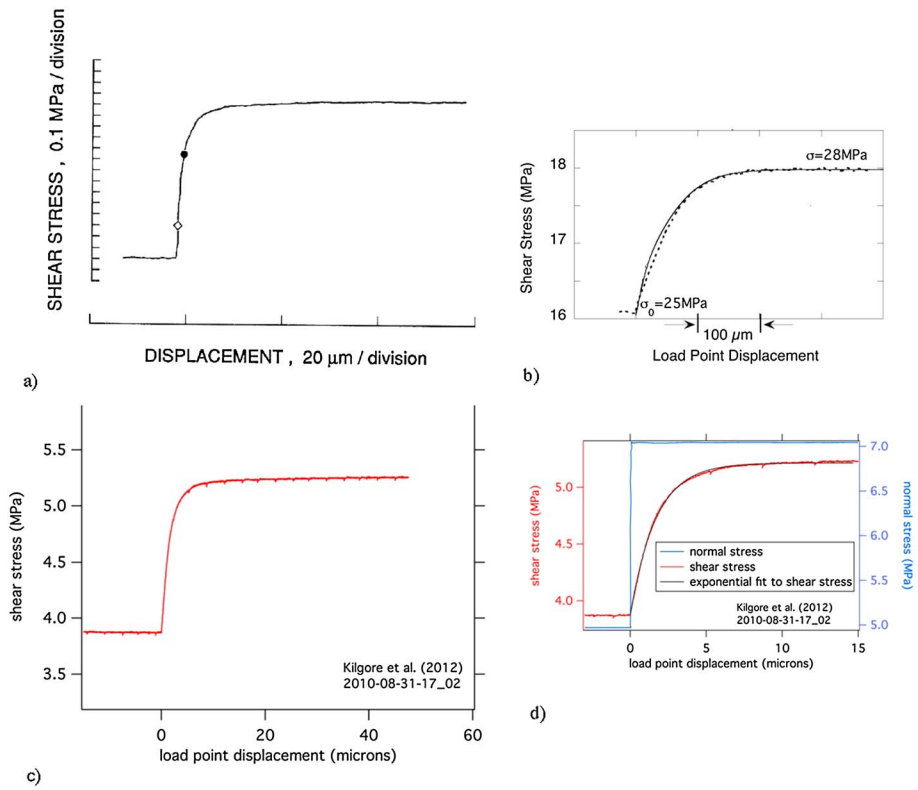

Figure 1. Normal stress steps in previous rock friction studies. (a) A 2 MPa step in normal stress on bare Westerly granite at 5 MPa initial normal stress and load point displacement rate of 1 μm/s, figure from *Linker and Dieterich* [1992]. The open and solid symbols mark the first two stages of the interpreted response (see text). (b) A 3 mm thick layer of quartz gouge at 25 MPa normal stress and load point displacement rate of 0.1 mm/s, figure from *Hong and Marone* [2005]. The dashed curve is data and the solid curve is a fit to the data using the two-stage *Linker and Dieterich* [1992] constitutive equations. (c) A 1 MPa step in normal stress on bare Westerly granite at 5 MPa initial normal stress and load point displacement rate of 1 μm/s from *Kilgore et al.* [2012]. (d) Same data as in Figure 1c (red), plotted at an expanded horizontal scale. In blue is the imposed change in normal stress (right axis). In black is an exponential fit to the shear stress (left axis) indicating a continuous, nonlinear, monotonic, response (see section 4.2).

instantaneously to step changes in the applied normal stress but gradually evolves to a new steady state level as a function of accumulated slip. *Prakash*'s [1998] tests were bimaterial interfaces of 4340 VAR steel or 6Al-4V titanium alloy samples, sliding against tungsten carbide targets. The interface slip velocities at the time of the normal stress change are extremely high at 1 to 30 m/s, as are the normal stresses, 500 to 3000 MPa. Because of experimental technique and the high slip rates used, the normal stress change is applied to the surface by an elastodynamic reflection, after the fault is already sliding at seismic or higher slip speeds, and thus, these results are not easily extrapolated to the problems of earthquake triggering or rupture propagation through geometric complexity. On the positive side, an important issue in application of experimental results to earthquake triggering and rupture propagation is resolving the immediate response of fault strength to changes in normal stress, requiring high data acquisition rates which for *Prakash* [1998] are not fully documented but greatly exceed a megahertz, perhaps approaching 1 GHz. Thus, these experiments were the first in which the immediate response of fault strength to changes in normal stress were examined at high resolution.

Most recently, in an effort to reconcile the rock friction observations [*Hobbs and Brady*, 1985; *Olsson*, 1988; *Linker and Dieterich*, 1992; *Hong and Marone*, 2005] with the constraints required by plausible physical models of dynamic rupture [*Rice et al.*, 2001; *Ranjith and Rice*, 2001], *Kilgore et al.* [2012] revisited the experimental approach of *Linker and Dieterich* [1992], using the same sample materials, sample preparation, testing procedures, and the very same testing machine but with two significant technical advances. First, through careful alignment and some good fortune, *Kilgore et al.* [2012] were able to essentially entirely eliminate the machine coupling between shear and normal stress in stress stepping experiments, thus removing the first stage in

Linker and Dieterich's [1992] and *Hong and Marone*'s [2005] observed response that overprints the fault's intrinsic behavior. Second, through the use of higher-resolution and higher-speed digital records, *Kilgore et al.* [2012] determined the immediate response of the shear resistance to changes in normal stress. Nonetheless, *Kilgore et al.*'s [2012] results of the response of fault shear resistance to a step increase in normal stress, if plotted at an equivalent time or displacement scale to the previous experiments of *Linker and Dieterich* [1992] (compare Figures 1a and 1c) or *Hong and Marone* [2005] (compare Figures 1b and 1d), are apparently identical. However, in detail (Figure 1d), the new study does not show the immediate linear increase in shear stress that follows the normal stress increase, which underlies all of the previous rock friction interpretations of the response. Instead, the evolution of shear stress is a gradual approach to steady state with slip, much as suggested by *Prakash* [1998].

The present study is an expanded analysis and a more comprehensive consideration of the complete suite of normal stress experiments that were in part described by *Kilgore et al.* [2012]. The expanded data set and analysis includes step decreases and increases in normal stress, the stability of slip following normal stress decreases, and the effects of normal stress pulse tests on fault strength. As a practical matter, though this is a study of friction, the dimensionless ratio of shear stress to normal stress, we typically will not examine changes in friction itself. Rather, much of our attention is focused on changes in shear resistance (with units of stress). This is because controlled changes in normal stress induce changes in friction that include both the cause of the change (normal stress) and the response (shear resistance). In other words, to understand friction in response to controlled changes in normal stress, it is easier to study the associated changes in shear resistance than in friction itself. An additional point of clarification is because our experiments are conducted at quasi-static conditions where inertial terms are negligible (see equation (B1a) in Appendix B below), we use the terms "shear resistance," "shear stress," and "shear strength" interchangeably throughout this report.

Besides detailed observations of the change in fault shear resistance, in this study the changes in fault normal closure and in the amplitude of small amplitude, high-frequency seismic waves transmitted across the fault are used to constrain the physical processes that determine the shear resistance. The goal of this study is to empirically establish the laboratory response of faults to changing normal stress and to develop a contact-scale physical model that accounts for the observations. As described above, the response influences seismic rupture arrest, earthquake initiation, and the estimates of the associated hazard. Determining the stability of slip and the changes in slip speed induced by reductions in normal stress are the key experimental observations necessary to apply lab results to dynamic rupture and earthquake triggering. Accordingly, we utilize laboratory observations to develop a conceptual model for physics-based earthquake initiation and rupture simulation as normal stress varies.

2. Experimental Methods and Measurements

The experiments were conducted in a servo-controlled, DDS testing apparatus [*Dieterich*, 1978] (Figure 2). The two faults of granite, consisting of side block surfaces measuring 5 cm × 5 cm and the 5 cm × 8 cm surfaces of the center block, were hand lapped with #60 silicon carbide abrasive and water on a glass plate. The resultant roughened surfaces were checked to be flat and parallel to within 0.025 mm. The apparatus permits servo control of sliding speeds from 10^{-4} μm/s to 10^{3} μm/s and of normal stresses up to 150 MPa. In the primary experiments the loading point slip rate is held constant at 1 μm/s and the normal stress is varied between 5 and 7 MPa. Slip rate and normal stress are controlled using a proportional-integral-derivative (PID) servo system to minimize overshoot, drift, and oscillation of the control. The proportional circuit linearly amplifies the error signal, the difference between a computer generated reference signal and the feedback signal from the sensor monitoring the control variable. Additional analog circuits integrate the error over recent history and take the derivative of the recent error signal. The controller uses a combination of the proportional, integral, and derivative response to the error signal to drive the servo valves that control the flow of oil into and out of the hydraulic cylinders which generate the normal and shear forces in the test apparatus.

2.1. Measurements

The primary experimental data are 16 bit digital records of the voltages from load cells measuring fault shear stress, normal stress, and from displacement sensors measuring fault slip and fault normal displacement across the interface. Data are saved at the rate of 100 pts/s (Hz). Each saved data point represents 10 data points recorded at 1000 Hz, averaged in real time.

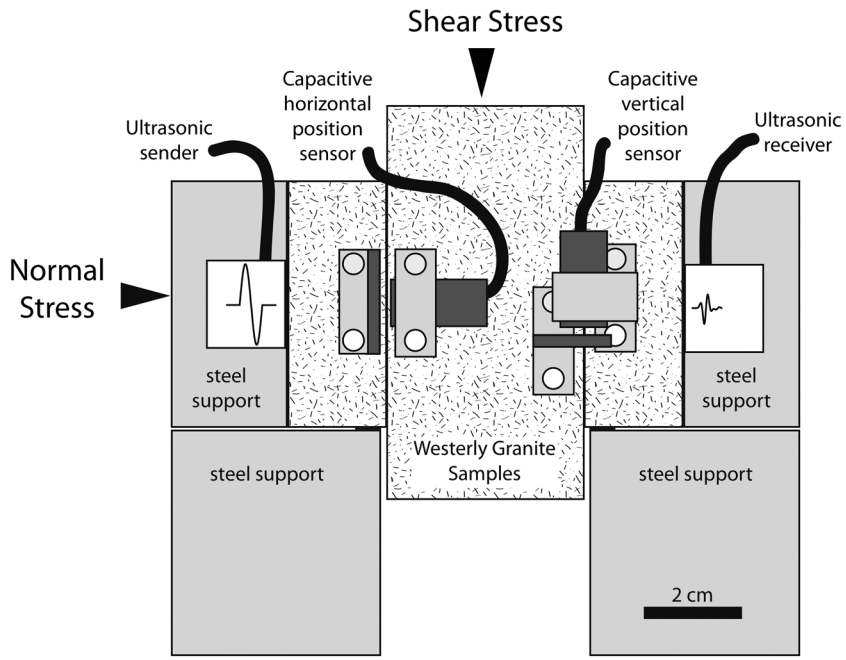

Figure 2. The biaxial experimental geometry used, consisting of applied shear and normal forces. Shear and normal stress are measured by load cells above and to the left, respectively, of the stress labels. Additional instrumentation includes a slip sensor, acoustic transmitter/receiver, and a fault normal displacement sensor.

2.1.1. Stress

Normal stress is servo controlled using the output from the horizontal load cell. The shear stress is a passive record of the vertical load cell output. The load cells are both 11,340 kg capacity. The nominal 5 MPa normal stress in these tests is about 1275 kg force and shear force in these tests is between 1656 and 2313 kg. Resolution of shear and normal stress are ±0.2 and 0.4 kPa, respectively.

2.1.2. Fault Slip/Load Point Displacement

Fault slip is measured using a small Lion Precision C2-A capacitive sensor paired with their RD22 driver modules with a response rate DC to 20 kHz. The sensor and its target are mounted on opposite sides of one of the faults in the DDS geometry. The slip sensor output resolution is ±0.1 μm. The servo-controlled system loading the fault uses fault slip as the feedback signal to control fault slip rate. The near-fault measurement minimizes compliance between the load point and the fault, thus maximizing the stiffness of the loading system. The recorded values of fault slip are better considered as the load point displacement of the testing machine and control system, including actual fault slip and a small amount of elastic distortion in the rock between the sensor mounting points. Actual fault slip can be estimated from this load point displacement, the known stiffness of the control system and the measured shear stress (see section 4.2).

2.1.3. Fault Normal Displacement

A displacement sensor, identical to the fault slip instrument, is mounted orthogonal to the fault surfaces to measure fault normal displacement across one of the faults in the DDS geometry at a resolution of ±0.030 μm. The fault normal displacement data have been corrected for linear compaction trend of ~0.001 μm/μm that results from wear of the fault surface or from misalignment of the sensor. The sensor mounts for these measurements are positioned similar to the fault slip sensor mounts, but with 3 mm more of cross fault distance between them. Accordingly, these measurements include more elastic distortion within the bulk, than for the fault slip measurements. Where necessary these changes have been removed from the measurements as follows. For a change in normal stress there is strain in the bulk of the same sense as the strain across the interface; that is, for an increase in normal stress there is compressive strain in the bulk and across the interface. The extraneous strain can be approximated by that resulting from a uniaxial stress change. Similarly, in the direct shear geometry an increase in average shear stress at the interface is accompanied by an increase in thickness of the fault blocks as measured normal to the interface. This correction can be approximated by the strain resulting from the Poisson effect of changing the loading stress. That is, we

treat both the normal and shear loading effects separately as due to uniaxial loading. Doing so is likely a very good approximation for the normal stress, as it is uniaxially applied. However, the shear stress is applied to the top of the center block uniaxially but is supported below by the stationary side blocks and the resulting stresses and strains due to this load are not uniform throughout the center and side blocks. Nonetheless, for simplicity we treat the average contribution as being equivalent to a uniaxial load. Fortunately, the shear stress is the smaller of the two corrections. In any case we believe the poorly known errors associated with the shear stress correction do not affect the conclusions of this study. The combined correction to the measured normal displacement δ_n is

$$\delta_n^{\mathrm{cor}} = \delta_n - \frac{L_n(\sigma_e - \sigma_0)}{E} + \frac{L_s \upsilon(\tau - \tau_0)}{E} \tag{1}$$

where L_n and L_s are the distances between the mounting points of normal (~14 mm) and shear (~11 mm) transducers and targets, respectively, E is Young's modulus (36 GPa), and v is Poisson's ratio (0.17) (values at 5 MPa uniaxial stress are from *Martin et al.* [1990]). σ_0 and τ_0 are arbitrarily chosen reference values of normal and shear stress which are taken to be the measured values prior to the imposed normal stress change. The corrections due to changes in normal stress in (1) are of the order of 0.39 μm/MPa. This bulk deformation of the samples in response to changes in normal stress, amplified by the distance between the fault normal displacement sensor mounts, is about 27% of the observed fault normal compaction measurements. That percentage may seem overly large, but the 14 mm of bulk sample between the sensor mounts can accommodate small, but measurable amounts of deformation compared to the deformation that the tens of microns of topography of the fault surface roughness can accommodate. The elastic distortions accompanying changes in shear stress are on the order of 0.05 μm/MPa, around 4% of the compliance.

2.1.4. Transmitted Amplitude and Fault Normal Stiffness

A separate data acquisition system records fault normal incident waves transmitted across the faults. The active seismic system uses a broadband *P* wave transducer with a central frequency of 1 MHz (Panametrics V103RM). The transducer element is 0.5 inches across. A 20 V peak to peak 1 MHz, single-cycle sine wave pulse is produced at the source transducer using a Tabor WW2572A waveform generator once every 0.01 s, resulting in an effectively continuously sampled record of the transmitted amplitude. After having propagated across the faults, the wave is detected by a second, identical transducer. The received signal is amplified and passed through a 300 kHz high-pass filter and a 5 MHz low-pass filter using a Panametrics 5800 Pulser/Receiver. The received sine wave pulses are digitized at the rate of 100 MHz with 14 bit of resolution.

After the experiments are completed the recorded waves are processed to determine the time history of transmitted amplitude. The relative amplitude of a wave transmitted across a single sliding surface, $|T|$, in this DDS geometry is

$$|T| = \sqrt{\frac{a_t}{a_0}} \tag{2a}$$

[*Nagata et al.*, 2008], where a_t is the measured amplitude of the received sine wave pulse traversing the entire sample assembly and a_0 is the amplitude of an identically sourced sine wave, traversing a single, solid block of Westerly granite that is the same thickness as the sample assembly. The difference between equation (2a) and the transmitted amplitude in an early study in this apparatus [*Nagata et al.*, 2014, equation (3)] is due to there being two fault surfaces in DDS and only one in the earlier study.

Since the acoustic waves are traveling elastic distortions, their transmitted amplitude is sensitive to the elastic properties of the interface and the bulk. The fault is an interface of elastic contrast relative to the surrounding material, having reflection and transmission coefficients commensurate with the magnitude of the contrast [*Kendall and Tabor*, 1971; *Schoenberg*, 1980; *Pyrak-Nolte et al.*, 1987, 1990]. The wavelength is large, ~5.5 mm, relative to the asperity contacts on the fault that in part determine the interface stiffness. By treating the fault as a displacement discontinuity, and attributing all the changes in transmitted amplitude to the contrast at

the interface, wave propagation theory relates the relative amplitude T of the transmitted wave to interface stiffness k as

$$k = \frac{k_*}{\sqrt{\frac{1}{|T|^2} - 1}}, \tag{2b}$$

[*Kendall and Tabor*, 1971; *Schoenberg*, 1980; *Pyrak-Nolte et al.*, 1987]. Here k is the specific interface stiffness, k_* is a constant $k_* = \omega\rho\beta/2$ where ω is angular frequency of the wave ($2\pi \times 10^6$/s in our experiments), ρ is density (2.63 g/cm^3 [*Martin et al.*, 1990]), and β is the elastic wave propagation speed (5486 m/s [*Martin et al.*, 1990]). For our experiments in granite k_* is 45.47 MPa/μm. At high frequencies $k_*/k \gg 1$ and T is proportional to the stiffness [*Yoshioka and Iwasa*, 2006]; nonetheless, we use the complete relation (2b) to convert normalized amplitude to stiffness throughout.

2.2. Tests

Three types of tests were performed to determine the effects of normal stress change on fault strength, sliding stability, fault dilatancy, and acoustic transmissivity across the fault: step increases, step decreases, and pulse tests. Normal stress steps determine the response of the fault to static stress changes. The step decreases establish the position of the sliding stability boundary. Transient step increases and decreases in normal stress were also performed whose purpose was to investigate effects of transients as during natural dynamic stress changes.

2.2.1. Step Increases

In the nominal step tests, increases in normal stress are imposed from a starting normal stress of 5 MPa, while the load point displacement rate is 1 μm/s. The size of successive increases are increments of 1, 2, 4, 5, 10, 20, and 40% of the starting value, corresponding to changes of 0.05, 0.1, 0.2, 0.25, 0.5, 1, and 2 MPa. The change is imposed as rapidly as possible without producing significant overshoot of the target normal stress. In practice the duration of the imposed change is less than 0.17 s. Normal stress is held constant at the target as the shear stress evolves to steady state. Successive step increases are separated by 100 μm of load point displacement. Half of that displacement is at the previous target normal stress and the remainder is at the starting value following a normal stress step decrease (see below). Additional step increases were conducted at sliding rates of 0.5 and 5 μm/s to determine the relative roles of time and slip in the evolution of shear strength and fault properties following a change in normal stress.

2.2.2. Step Decreases

The step decreases are of the same size as the increases, are at the same load point displacement rate of 1 μm/s, and are interspersed with the increases. They are returns to the nominal normal stress of 5 MPa. For purposes of control the decrease in normal stress is imposed somewhat more slowly than the increase. Because the machine stiffness results from servo control and depends on resolving fault displacement, if the normal stress is decreased too quickly, the control system is dynamically less stiff. In practice, the duration of the imposed change occurs in less than 0.3 s. Normal stress is then held constant at the target as the shear stress evolves to steady state. Successive step decreases are separated by 100 μm of load point displacement. Half of that displacement is at nominal level and the remainder is at the previous step increase target normal stress.

2.2.3. Pulse Tests

Like the step increases, the pulse tests are imposed from a starting normal stress of 5 MPa and load point displacement rate of 1 μm/s. The size and succession of pulses are intended to be the same as for the step tests. The normal stress increase is imposed over less than 0.07 s. Normal stress is then held approximately constant for 0.2 s total duration and returned to the starting normal stress in around 0.1 s. Successive pulse tests are separated by 50 μm of load point displacement.

3. Experimental Results

For each of these tests (step increases, pulse tests, and step decreases) the observed changes in transmitted amplitude, shear strength, and fault normal displacement are described in detail in the following subsections. The static stress increases document a stable slip response, an increase in shear resistance, fault closure, and

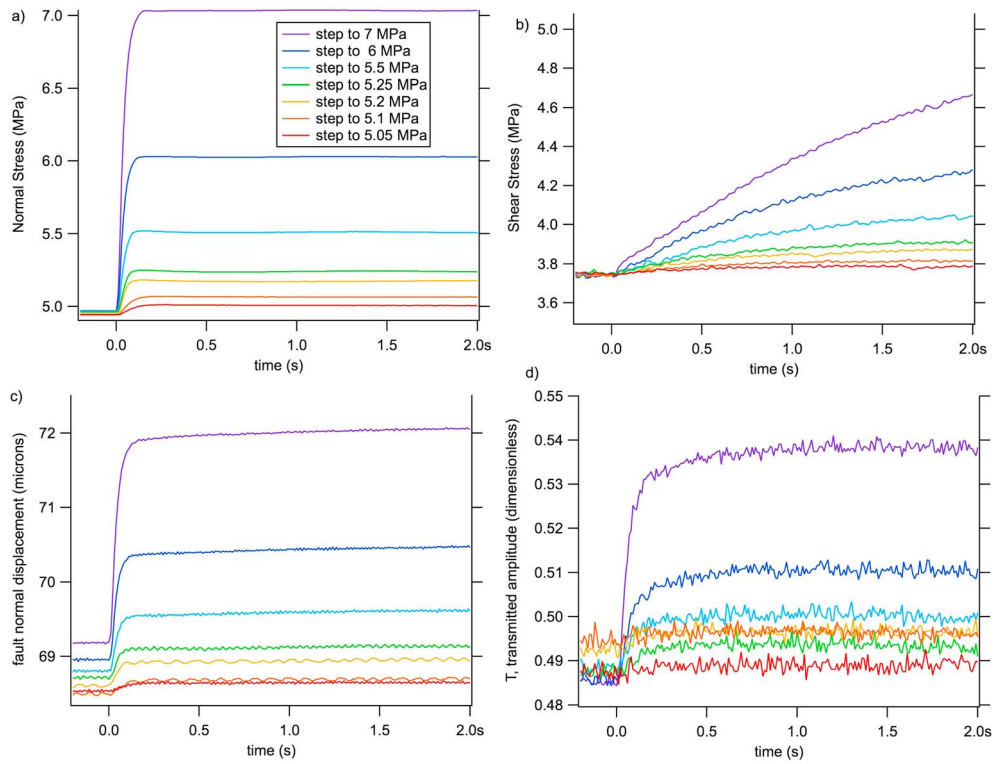

Figure 3. Scaled normal stress step increase data. Size of the stress change is indicated in the legend in Figure 3a and the same color coding of the steps is used in Figures 3b–3d. (a) Normal stress. (b) Shear stress. (c) Fault normal displacement, not corrected for displacement trend or for elastic coupling equation (1), see text. (d) Dimensionless transmitted amplitude from equation (2a) with a_0 = 3.85 V.

an increase in fault normal stiffness. The pulse tests produce stable response of fault slip. Step decreases show dilatancy, reduction in fault stiffness, and, depending on the size of the step, stable or unstable responses of the shear stress, providing constraints on the location of the stability boundary.

3.1. Step Increases

Two sets of steps were conducted at the nominal sliding rate of 1 μm/s; one complete suite of data from the step increases are shown in Figure 3 after *Kilgore et al.* [2012]. The traces are color coded to indicate the size of the stress step. For shear stress, fault normal displacement, and transmitted amplitude, the size of the response scales systematically with the size of the imposed change in normal stress. The details of the responses differ, however. Shear stress (Figure 3b) shows a prolonged evolution. In contrast, the fault normal displacement response is nearly identical to the imposed change in normal stress and shows nearly no evolution with displacement or time (Figure 3c). Transmitted amplitude (Figure 3d) shows a response that is intermediate between the shear stress and fault normal displacement. Most of the response tracks the normal stress change immediately, but with a small amount of evolution with time. The evolution distance is much shorter than that for shear stress.

3.2. Step Increases at Different Loading Rates

To distinguish whether the evolution of fault properties following a normal stress increase results from time- or slip-dependent evolution, similar tests were conducted at lower and higher slip speeds (Figures 4 and 5) [*Kilgore et al.*, 2012]. Step increases and decreases were conducted on the same samples at lower and higher load point displacement rates of 0.5 μm/s and 5 μm/s. One suite of step tests at the lower rate increases are shown in Figure 4. In these tests the apparent evolution time for shear stress is longer than in the tests at 1 μm/s slip rate (compare with Figure 3b), consistent with the evolution being due to slip rather than time. The same can be said for the evolution of transmitted amplitude which is longer at the lower slip rate. One suite of step increases at 5 μm/s is shown in Figure 5. Again,

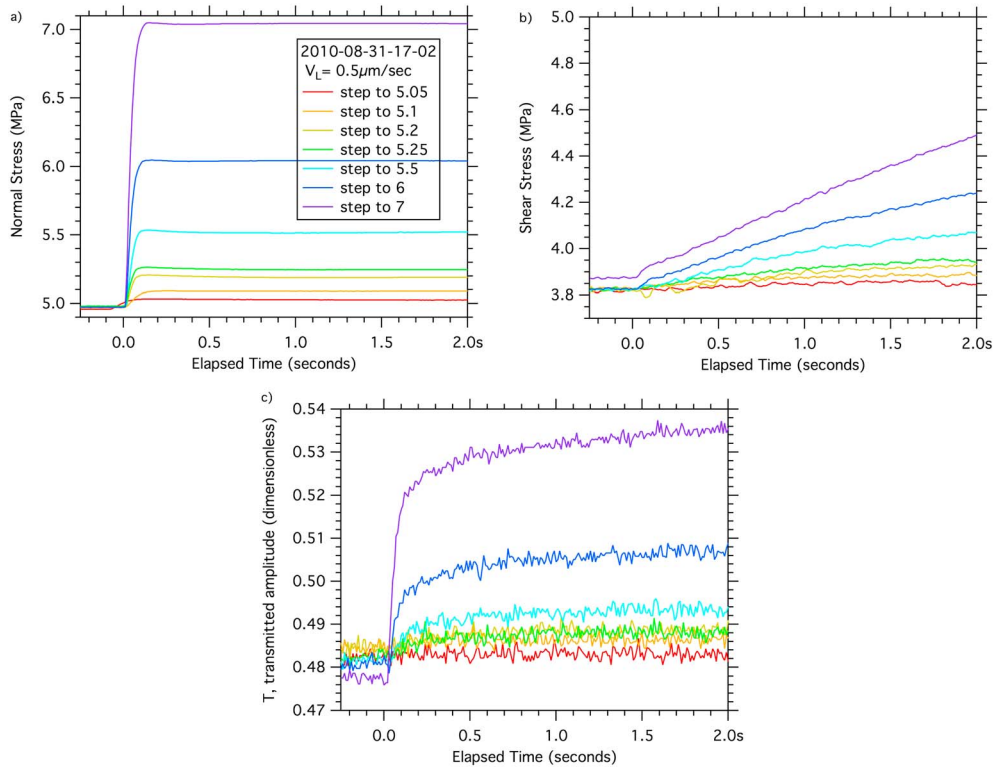

Figure 4. Scaled normal stress step increase data at loading velocity of 0.5 μm/s. Size of the stress change is indicated in the legend in Figure 4a and the same color coding of the steps is used in Figures 4b and 4c. (a) Normal stress. (b) Shear stress. (c) Dimensionless transmitted amplitude from equation (2a) with a_0 = 3.85 V.

consistent with slip evolution, shear stress and transmitted amplitude changed more rapidly with time at this higher slip rate. Fault normal displacement was not recorded in any of the tests at the lower and higher slip rates because the sensor was off-line. Superimposing the shear stress evolution during steps from 5 MPa to 6 MPa at all three load point displacement rates versus load point displacement rather than time (Figure 6a) shows the displacement length scale more clearly and indicates the response is independent of the loading rate and governed by slip evolution. A similar plot of the evolution of transmitted amplitude (Figure 6b) also lacks a dependence on loading rate and evolves with slip. Noting that the displacement scale differs in Figures 6, transmitted amplitude changes with a much shorter characteristic displacement than for the shear resistance.

3.3. Pulse Tests

Six sets of pulses were conducted; one complete suite of scaled experimental data is shown in Figure 7. In the figure, as with step increases, the traces are color coded to indicate the size of the stress pulse. There are some minor control issues during the duration of the pulse where ideally the normal stress would be held perfectly constant. As is clear in Figure 7, there are slight decreases in the normal stress during this time. The responses are mostly consistent with those observed for the step increases, namely, the size of the response scales systematically with the size of the imposed change in normal stress and the details of the responses differ. Keep in mind that direct comparisons with the step tests are appropriate for the increasing stage of the pulse as these start from the same initial condition as a step increase, but during the decreasing stage of the pulse the fault is in a nonsteady state condition, unlike that for the step decreases.

Nonetheless, with a few exceptions shear stress (Figure 7b) shows the same slow response to the increase in normal stress. A slow decrease follows the decrease in normal stress. The largest two pulses show evidence of a more rapid decrease which may be due to accelerated slip, and the very largest pulse shows a nonmonotonic decay, possibly influenced by arrest of rapid slip by the control system but more likely due to unwanted coupling of shear to normal stress such as seen in the earlier *Linker and Dieterich* [1992] study. Again, the fault

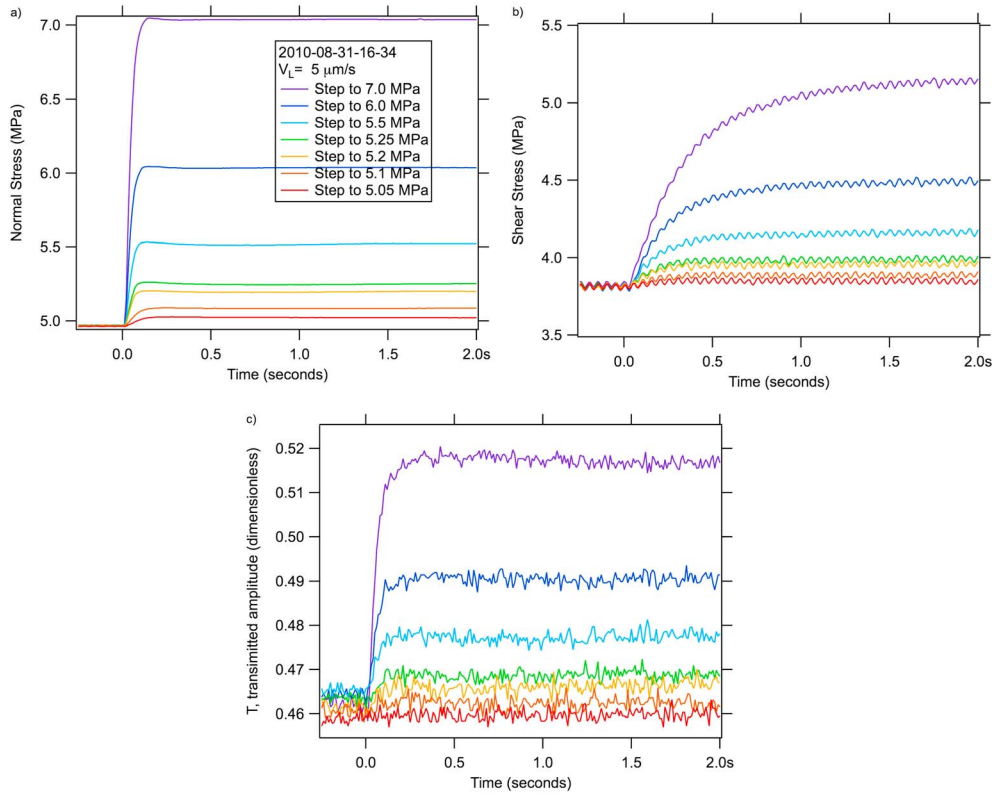

Figure 5. Scaled normal stress step increase data at loading velocity of 5 μm/s. Size of the stress change is indicated in the legend in Figure 5a and the same color coding of the steps is used in Figures 5b and 5c. (a) Normal stress. (b) Shear stress. (c) Dimensionless transmitted amplitude from equation (2a) with a_0 = 3.85 V.

normal displacement response is nearly identical to the imposed change in normal stress (Figure 7c). Most of the compaction that occurs during the normal stress increase is recovered in the stress decrease. There is a relatively small offset of the baseline displacement for the largest pulses. Unlike the shear stress, there is no clear change in the form of response as the size of the pulse is increased, notably no change for the very large decreases where shear stress shows complications likely due to rapid changes in slip speed. As for the step increases, the transmitted amplitude (Figure 7d) shows a response that is intermediate between the shear

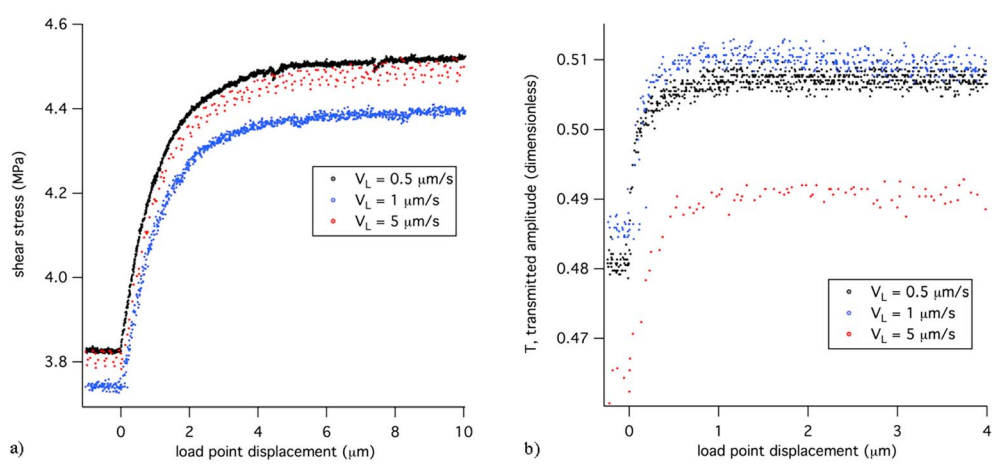

Figure 6. Comparison of the evolution of fault properties with slip. (a) Shear stress from loading rates of 0.5, 1, and 5 μm/s for normal stress steps of 1 MPa plotted versus load point displacement. (b) Transmitted amplitude for the same steps as shown in Figure 6a.

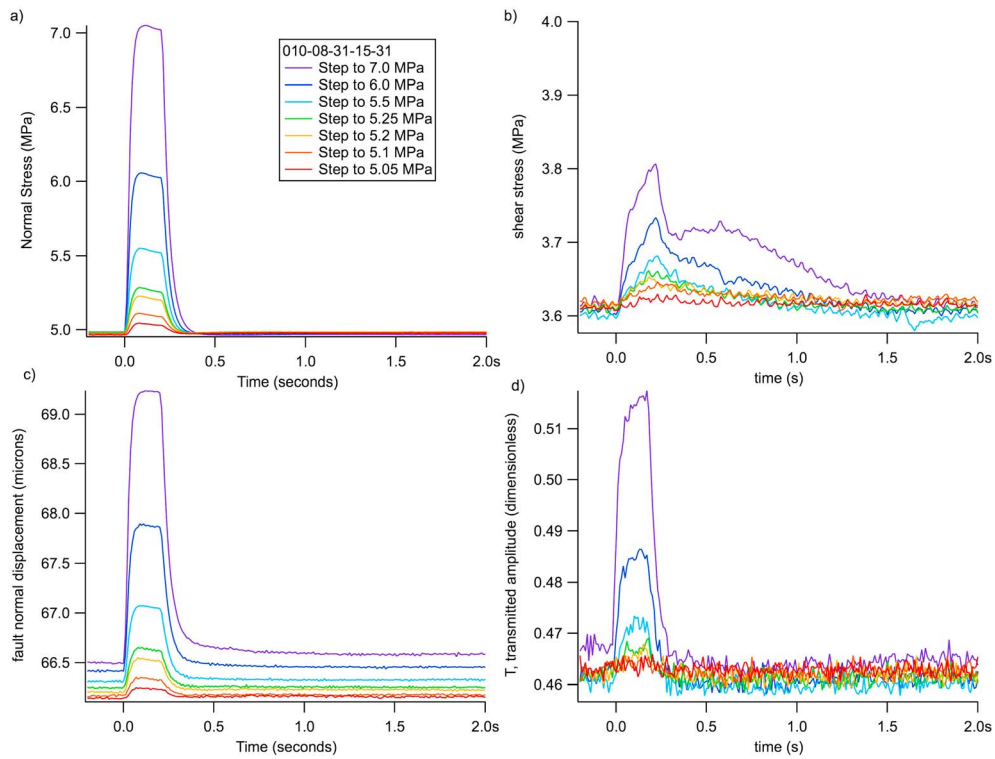

Figure 7. Scaled normal stress pulse test data. Size of the stress change is indicated in the legend in Figure 7a and the same color coding of the steps is used in Figures 7b–7d. (a) Normal stress. (b) Shear stress. (c) Fault normal displacement, not corrected for displacement trend or for elastic coupling equation (1), see text. (d) Dimensionless transmitted amplitude from equation (2a) with A_i = 3.85 V.

stress and fault normal displacement. Most of the response tracks the normal stress change immediately, but with a small amount of evolution with displacement while the normal stress is briefly held approximately constant. Then when the normal stress is decreased, most of the offset is recovered immediately. Whatever transient response there is upon the normal stress decrease would seem to have a shorter time or slip evolution distance than for the increase and shorter still than the shear stress.

3.4. Step Decreases

Two sets of step decreases were conducted; one complete suite of scaled experimental data is shown in Figure 8. As in prior plots the traces are color coded to indicate the size of the stress step. Shear stress step decreases of up to 0.5 MPa show a stable but rapid decrease in shear resistance (Figure 8b). The evolution distance is much shorter than in step increases, at least in part due to slip acceleration accompanying the normal stress decrease. Steps of 1 MPa or larger are unstable. As for the step increases and pulse tests, the fault normal displacement response is nearly identical to the imposed change in normal stress and shows little evolution with displacement or time (Figure 8c). The transmitted amplitude during the smallest stable down steps (Figure 8d) tracks the normal stress decrease directly with perhaps a small amount of evolution with time. For the larger stable and the two unstable steps there is a rapid decrease and overshoot of the final value by an amount that increases with the size of the down step.

4. Data Analysis and Physical Interpretation

Kilgore et al. [2012] presented an empirical interpretation of the same step increase data shown in Figure 3, namely, that while there are rapid changes in fault zone properties with normal stress (transmitted amplitude and closure), the shear resistance instead evolves gradually with displacement. Furthermore, because the tests were done at higher resolution in the same machine and conditions as the prior study, in the remainder of this study we assume that our empirical description supplants the two-stage shear stress response inferred

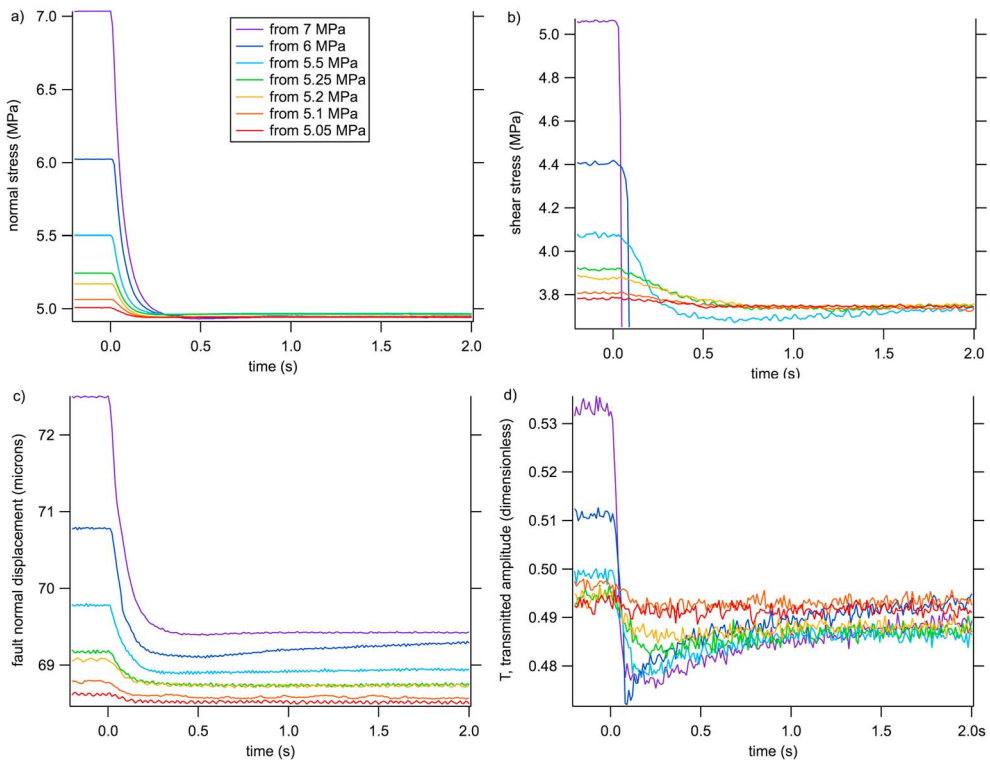

Figure 8. Scaled normal stress step decrease data. Size of the stress change is indicated in the legend in Figure 8a and the same color coding of the steps is used in Figures 8b–8d. (a) Normal stress. (b) Shear stress. (c) Fault normal displacement, not corrected for displacement trend or for elastic coupling equation (1), see text. (d) Dimensionless transmitted amplitude from equation (2a) with a_0 = 3.85 V.

from the experiments of *Linker and Dieterich* [1992]. Because those observations were the empirical motivation for the two-stage rate and state constitutive relations developed by *Linker and Dieterich* [1992] in which a parameter α is used to scale instantaneous changes in fault properties as normal stress is changed [*Linker and Dieterich*, 1992], and because our data provide no such evidence, we will also not discuss that constitutive model in this report. This should not be interpreted to imply that our data preclude instantaneous changes in fault strength or "state" as normal stress is changed. Indeed, it is well known that the *Linker and Dieterich* [1992] constitutive model can produce a gradual evolution of shear stress while state changes instantaneously with normal stress [*Bhattacharya et al.*, 2016].

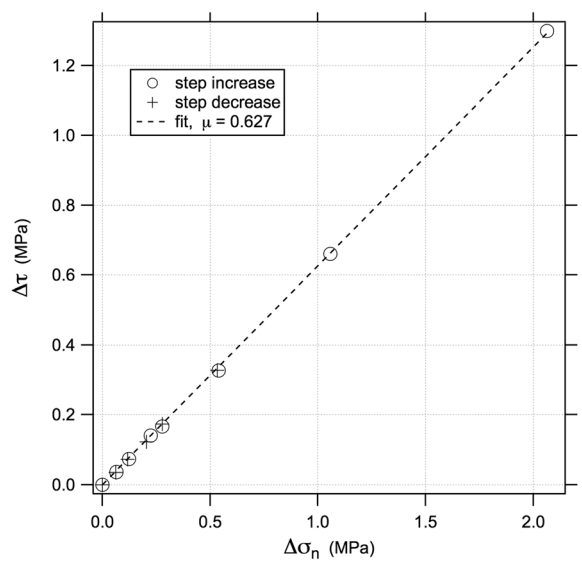

Figure 9. Steady state changes in shear stress resulting from normal stress step tests, here plotted versus the normal stress change. The slope of the fit (dashed) is the friction coefficient, μ = 0.63.

These issues with existing constitutive relations are beyond the scope of this study. In the following section we further analyze the step increase,

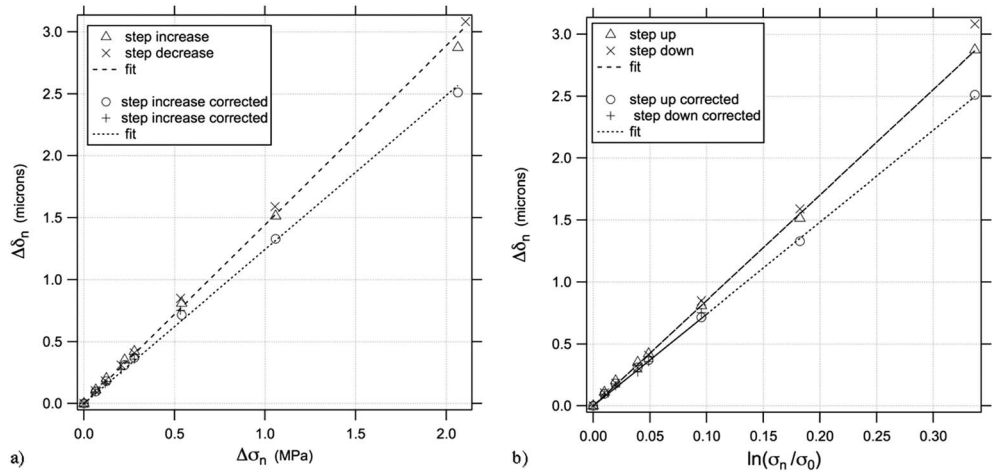

Figure 10. Steady state closure in normal stress step tests. (a) Closure versus normal stress change. Data corrected for stress change using equation (1) are open circles (step increases) and plus symbols (step decreases). The data fits have slopes of 1.4 (uncorrected) and 1.2 μm/MPa (corrected). (b) Closure versus natural logarithm of normal stress using the same symbols as in part Figure 10a. The data fits have slopes of 8.5 (uncorrected) and 7.4 μm (corrected) per unit natural log of dimensionless stress.

and also the step decrease and pulse test data to develop a physical interpretation of the response of faults to normal stress changes. The analysis initially expands upon the step data, first using the changes in the steady state conditions and then the transient changes. The pulse data and step decreases are subsequently used to further confirm or deny and refine the interpretation.

4.1. Steady State Response

The ratio of the net, steady state change in shear stress with normal stress during frictional sliding is the friction coefficient, which is shown in Figure 9, well defined to be 0.63 by the collective step increases and decreases, open symbols and crosses, respectively, in the figure. These values result from differencing the average shear and normal stress in the quarter second prior to the stress step and the average once the shear stress has reached steady state, the value between 18 and 20 s following the step. These same choices are used consistently for transmitted closure and amplitude in the analogous Figures 10 and 11.

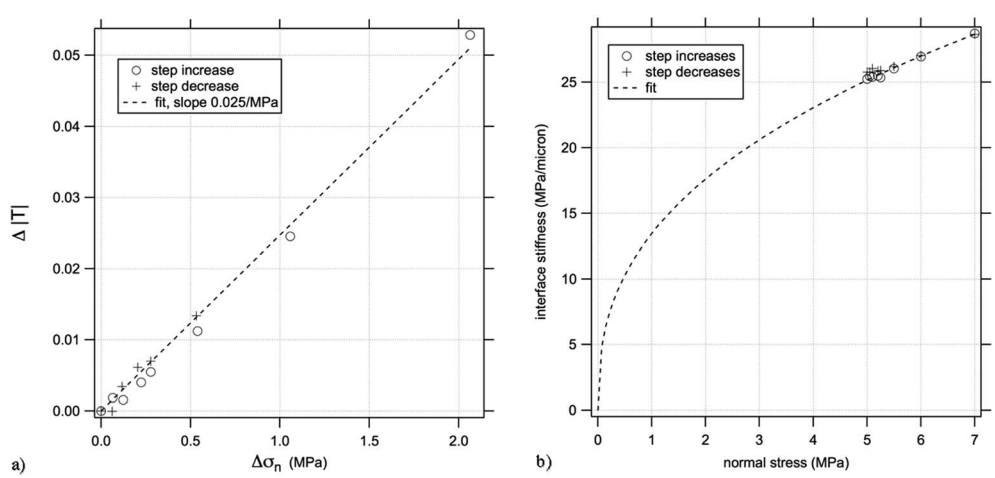

Figure 11. Steady state elastic properties of the fault from *p* wave transmission. (a) Change in transmitted amplitude versus normal stress change. Dashed line is a fit with slope 0.023/MPa. (b) Inferred specific fault normal stiffness from the transmitted amplitudes, equation (2b), versus normal stress. Dashed curve is a power law fit to the data with equation (4) and σ_0 = 5 MPa, k_0 = 25.14 MPa/μm, and n = 0.39.

The steady state closure measurements (Figure 10a) demonstrate the fault normal deformation associated with step changes in normal stress. The figure shows the response to step increases with (open circles) and without (open triangles) the stress correction, equation (1). There is some hysteresis between those measurements and the step decreases (plus signs and crosses). Despite the complication and the uncertainty associated with the stress correction, at least over the narrow, 2 MPa range of normal stresses considered, the steady state closure is approximately linear in normal stress. Not knowing at this stage in the analysis what processes are involved in determining closure, the following discussion considers possible interpretations of these data as linear and nonlinear dependences on normal stress, and physical models for these dependences. An approximately linear relation between fault normal stress and fault closure is expected under many circumstances. For example, the ratio of normal stress change to closure, the inverse of the slope in Figure 10a, is the static fault normal stiffness. Were all the deformation linearly elastic, the fault normal displacement versus normal stress data would resemble Figure 10a. Similarly allowing for some inelastic deformation, taking the shear stiffness of the interface $k_s = \mathrm{d}\tau/\mathrm{d}\delta_s$, the friction coefficient $\mu = \mathrm{d}\tau/\mathrm{d}\sigma_n$, and the dilation coefficient $D = \mathrm{d}\delta_n/d\delta_s$ [e.g., *Sleep*, 1997, 2006] to all be constants, then the slope in Figure 10a would be the constant, $\mu D/k_s$.

A more likely expectation from elasticity is that the deformation occurs preferentially in the region of asperity contacts leading to a nonlinear dependence of closure on normal stress [e.g., *Nagata et al.*, 2014]. For an analog material and larger (nearly zeroth order) relative changes in normal stress, the relationship between closure and normal stress is semilogarithmic [*Nagata et al.*, 2014]. Figure 10b shows our granite data versus the natural logarithm of normal stress, and it is also consistent with the *Nagata et al.* [2014] interpretation. Observational data [*Goodman*, 1976; *Brown and Scholz*, 1985] and theoretical arguments from elastic models of rough surfaces in contact based on *Greenwood and Williamson* [1966] [*Brown and Scholz*, 1985; *Yoshioka*, 1994] suggest generally that fault normal displacement depends logarithmically on normal stress, independent of the details of the contact-scale elastic interactions. The standard explanation for this is from *Greenwood and Williamson* [1966] who suggested that the distribution of asperity heights in contact on a frictional surface at any given load can be well approximated by an exponential function. This holds for many natural and laboratory rock surfaces [*Walsh and Grosenbaugh*, 1979; *Swan*, 1983; *Power and Tullis*, 1992]. Following these prior studies, the exponential height distribution leads to the same relation between normal displacement and normal stress, independent of the details of the elastic asperity compliance [*Beeler and Hickman*, 2001], the logarithmic variation

$$\delta_n = \delta_0 + c \ln \frac{\sigma_n}{\sigma_0}. \tag{3}$$

Here δ_0 is the fault normal displacement at the reference normal stress σ_0. In Figure 10b $\Delta\delta_n$ is $\delta_n - \delta_0$, where the reference is taken at the starting normal stress of $\sigma_0 = 5$ MPa in all the tests. In addition to being consistent with the observed relation between closure and normal stress (Figure 10b), equation (3) is the empirical relationship often used to relate normal stress to elastic joint normal displacement [*Goodman*, 1976]. The physical explanation of (3) for rough surfaces in contact is as follows: as normal stress is increased, the separation between the surfaces decreases resulting in increased strain at each contact, as graphically demonstrated in Figure 6a of *Dieterich and Kilgore* [1994]. In addition, other asperities come into contact as the separation decreases. Thus, for an increase in normal stress there are changes in the area of contact due to two effects: increase in area of the existing contacts and increase due to new contacts being created as fault closes. As shown in *Greenwood and Williamson* [1966] the elastic resistance to normal displacement arises primarily from the latter effect (the changing number of asperities in contact) that is controlled by the statistics of the asperity population, rather than the details of the elastic behavior of the asperities themselves. This is our favored interpretation, and we will return to the physical basis of closure when we consider the transient measurements. Nonetheless, these data clearly do not distinguish between logarithmic (Figure 10b) and linear (Figure 10a) dependence on normal stress, and this is an important issue for extrapolation to natural faults that should be resolved in subsequent studies conducted over a wider range of normal stress.

The change in transmitted amplitude is approximately linear in normal stress change over the narrow range of the measurements (Figure 11a). At step changes of less than 0.1 MPa, the relation is not well resolved for the step increases. This is due to a signal to noise limit in the transmitted amplitude measurements. The

overall regression indicates a weak dependence on normal stress, 0.023/MPa. There are some expectations for a linear relationship between transmitted amplitude and normal stress. For example, from equation (2b) at high frequency the transmitted amplitude and specific fault normal stiffness are proportional, while the static fault normal stiffness (the reciprocal of the derivative of (3) with respect to normal stress) from the rough surface contact model discussed above is proportional to normal stress [*Nagata et al.*, 2014]. In detail, however, the stiffness inferred from the measurements of transmitted amplitude and that implied by the static closure measurements are quite different. The linear stiffness defined by the static measurements is approximately 0.7 MPa/μm (Figure 10a), whereas the inferred interface stiffness for granite is much higher (see below). This discrepancy could relate to the differences in measurement method and frequency, but its origin is not known, and an explicit theory that relates closure and transmitted amplitude measures remains to be developed.

Nonetheless, of more relevance to the physics of friction is the relation between the transmitted amplitude and contact area. Theory suggests some kind of nonlinear relationship, for example, *Kendall and Tabor* [1971], where stiffness is proportional to the square root of contact area [also see *Balik and Thompson*, 1984]. Support for this requirement can be illustrated for our data set by converting the transmitted amplitude to fault normal stiffness using equation (2b) and plotting the result against normal stress, that is, using normal stress as a proxy for contact area (Figure 11b). Noting that at zero normal stress contact area and fault stiffness should both approach zero (zero contact, infinite compliance), the observations diverge significantly from a linear relation that includes the origin. Shown for reference is a simple power law fit,

$$k_n = k_0 \left(\frac{\sigma_n}{\sigma_0}\right)^n, \tag{4}$$

that is qualitatively consistent with the requirement of nonlinearity. In (4) k_0 is the static normal stiffness at the reference normal stress σ_0. In Figure 11b, $\sigma_0 = 5$ MPa, $n = 0.39$, and $k_0 = 25.14$ MPa/μm.

For friction the increase in steady state shear resistance with normal stress during sliding is well understood to result from an increase in contact area, due either to contact-scale yielding [*Bowden and Tabor*, 1950] or elasticity [*Greenwood and Williamson*, 1966]. The contact area increase has been shown quantitatively for transparent minerals and an analog material, lucite, over this range of normal stress in this apparatus at room temperature [*Dieterich and Kilgore*, 1994, 1996]. The change in shear strength with normal stress also implies elastic or inelastic normal strain between the fault surfaces as the normal stress is changed. This is another standard expectation from classic studies of brittle deformation and frictional sliding [*Brace et al.*, 1966; *Escartin et al.*, 1997, 2008], namely, that frictional slip requires dilatancy. Accordingly, the increasing steady state shear resistance with normal stress is the signature of an increase in volumetric or fault normal work done against the confining stresses, necessary to allow shear deformation. And the changes in contact area imply changes in the fault normal stiffness. Thus, each of the steady state changes in shear strength (Figure 9), fault normal displacement (Figure 10), and fault normal stiffness (Figure 11) with normal stress change are consistent with reversible changes in contact area, as expected from theory [*Bowden and Tabor*, 1950; *Greenwood and Williamson*, 1966]. Accordingly, it is nearly uniformly agreed that during frictional sliding the steady state shear resistance is proportional to the fractional contact area A

$$\tau \propto A \tag{5}$$

[e.g., *Dieterich*, 1979].

4.2. Transient Response

Equation (5) has been widely applied to nonsteady state conditions and underlies nearly all applications of laboratory rock friction to faulting and earthquakes (rate and state friction [*Dieterich*, 1979; *Ruina*, 1983; *Nakatani*, 2001; *Nagata et al.*, 2012]). Indeed, contributions of contact area are the basis of both of the prominent constitutive models of friction under variable normal stress [*Linker and Dieterich*, 1992; *Prakash*, 1998]. In the Linker and Dieterich model, rapid changes in normal stress induce immediate changes in contact area, therefore in state [*Linker and Dieterich*, 1992] and, in some model implementations, very large changes in

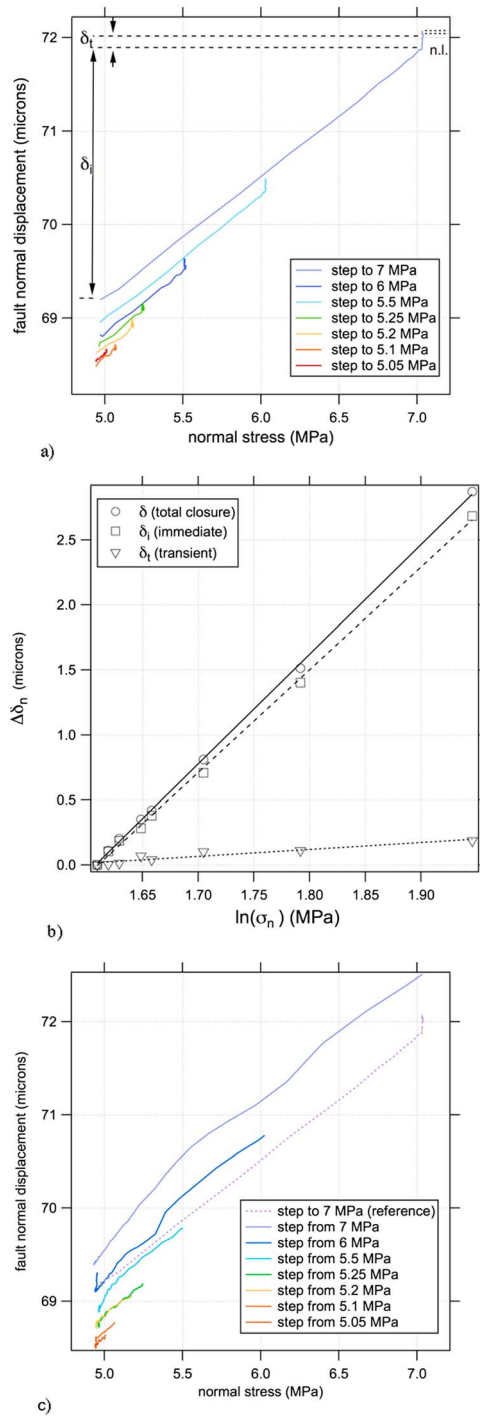

Figure 12. Transient fault normal displacement. (a) Records of normal displacement versus normal stress in the first 2 s following step increases in normal stress. The fault normal displacement records consist of two stages: a large immediate, linear response labeled δ_i for the step between 5 and 7 MPa (purple), followed by a very small transient labeled δ_t. The noise level on the displacement during sliding at state-state is labeled n.l. The noise is defined as the maximum and minimum recorded values between 1.75 and 2 s. This level is essentially the same for all steps. (b) Reduced values of total, immediate, and transient response for the cases shown in Figure 12a, here plotted versus natural logarithm of the target normal stress. (c) Same as Figure 12a but for step decreases in normal stress.

slip speed. Similarly in Prakash's interpretation, though his observations indicate that rapid changes in normal stress do not produce large immediate changes in slip speed, the observed gradual change in shear resistance with slip is interpreted as resulting from an underlying gradual change in contact area [*Prakash*, 1998]. In contrast to these prior data and interpretations, and as detailed in the following analysis, the most straightforward interpretation of the transient response to changes in normal stress in the present study, is that they preclude the strict physical interpretations of Prakash and Linker and Dieterich, though aspects of both are involved. In this section we first describe the transient response of fault normal displacement, transmitted amplitude, and shear stress and then discuss their constraints on physical models of fault properties.

To illustrate the transient response to changes in normal stress, normal displacement, transmitted amplitude, and shear stress from the normal stress step increases (Figures 3c, 3d, and 3b) are replotted versus normal stress rather than time. In the cases of normal displacement and transmitted amplitude the responses can be divided empirically into two stages. For example, Figure 12a shows the step changes in fault normal displacement, using the same color coding as in the original figure, a convention that is adhered to throughout. These are records of normal displacement versus normal stress in the first 2 s following the step for the seven-step increases in normal stress. To illustrate the data reduction and definition of the two stages, there is a large intermediate, linear response labeled δ_i for the step between 5 and 7 MPa (purple), followed by a very small transient labeled δ_t. To quantify the sizes of each contribution, for each step the displacement from the onset to the

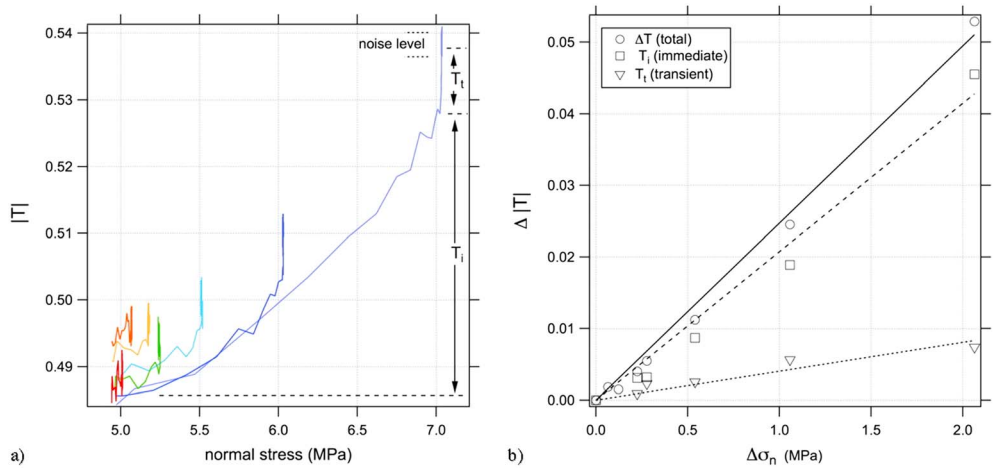

Figure 13. Transient transmitted amplitude. (a) Records of transmitted amplitude versus normal stress in the first 2 s following step increases in normal stress. The records consist of two stages: a large immediate response labeled T_i for the step between 5 and 7 MPa (purple), followed by a smaller transient labeled T_t. (b) Reduced values of total, immediate, and transient response for the cases shown in Figure 13a, here plotted versus the target normal stress.

abrupt change in slope is measured as δ_i and from that point to the steady state value is δ_t. The total closure is defined by the average between 1.75 and 2 s since the onset, as indicated by the schematic definitions on the figure. The approximate noise amplitude is also labeled n.l. on the figure. Values of the immediate and transient responses are shown in Figure 12b along with the total amount of closure associated with each step. Reference lines are fits to the data. Approximately 94% of the fault normal displacement is immediate. Normal displacement in response to the step decreases in stress is more complicated (Figure 12c). Similarities are that the initial expansion associated with step decreases is linear and has the same slope as for the step increases; the largest step increase in Figure 12a is shown for reference in Figure 12c. A reasonable interpretation is that the immediate normal displacement δ_i is elastic displacement, as seems to be required by its association with the rapid change in stress and its reversibility. The principal complication in the step decreases is a deviation from the well-defined two stage response for the two largest steps. Because rapidly accelerating slip and instability is associated with these steps, the deviation is expected based on prior studies of rate dependent dilatancy [*Marone et al.*, 1990; *Marone and Kilgore*, 1993]. That is, so long as the slip rate during the step increases remains close to the load point displacement rate, the two-stage response to rapid normal stress changes can be interpreted as an elastic normal stress-dependent and slip rate-independent effect followed by inelastic contribution controlled by a process that depends both on normal stress and slip rate, for example, plastic yielding at asperity contact on a sliding surface [*Scholz and Engelder*, 1976]. For step decreases in which the slip rate accelerates significantly the two effects will be superimposed rather than apparently sequential.

The transient behavior of transmitted amplitude (Figures 13a and 13b) is qualitatively similar to fault normal displacement, a two-stage response, and we use the same scheme to define the immediate and transient responses. The majority of the signal is immediate, approximately 85% (Figure 13b). There are some notable differences betweeen transmitted amplitude and normal displacement; in particular, the relationship of transmitted amplitude with normal stress during the immediate response is distinctly nonlinear. It is known empirically from prior experiments on transparent analog material, lucite plastic, that contact area and fault normal displacement are not tracked linearly by transmitted amplitude during step changes in normal stress [*Nagata et al.*, 2014], so this may be a related example. Though the physical reason for the nonlinearity is not known, nonlinear relations between contact area and stiffness are expected from elastic contact and crack models [*Kendall and Tabor*, 1971; *Balik and Thompson*, 1984]. Another stronger difference is the significant transient excursion and recovery in the transmitted amplitude during unstable slip (Figures 8c and 8d) that is not present or is muted in fault normal displacement. Based on this comparison, we conclude that the immediate response in granite is elastic and that the smaller transient

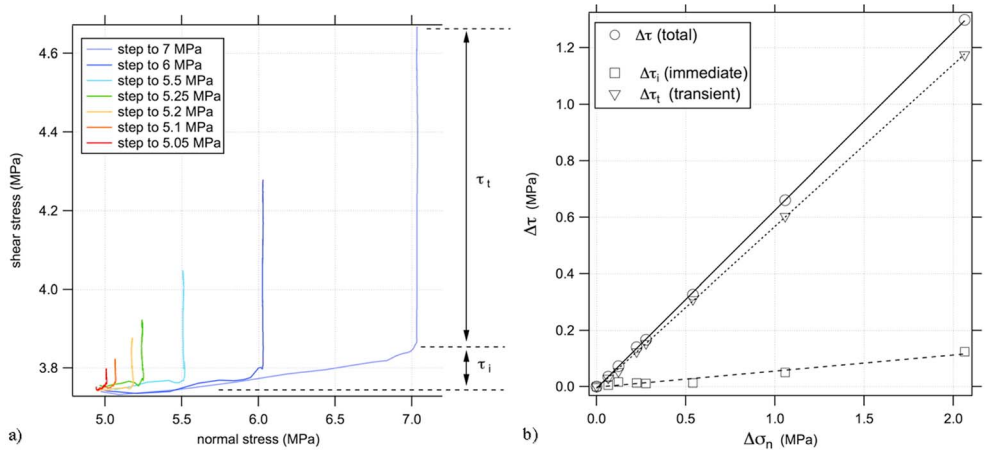

Figure 14. Transient shear stress. (a) Records of shear versus normal stress in the first 10 s following step increases in normal stress. The records consist of two stages: a small immediate response labeled τ_i for the step between 5 and 7 MPa (purple), followed by a larger transient labeled τ_t. (b) Reduced values of total, immediate, and transient response for the cases shown in Figure 14a, here plotted versus the target normal stress.

change is both normal stress and slip rate dependent, resulting from an inelastic process such as contact-scale yielding.

In contrast, when the first 2 s of the shear stress responses are plotted in the same way as in Figures 12 and 13, the immediate and transient responses show the opposite sense of the fault normal displacement and transmitted amplitude, with a small immediate and larger transient response (Figure 14a). The contrast between Figures 12/13 and 14 illustrates some of the inherent difficulties of interpreting the response to normal stress changes that occur over some finite duration. For instance, while the simplest interpretation of the shear stress time series in response to step increases (Figure 3) is that it follows a single continuous stage, in Figure 14a the same data could instead be interpreted as a two-stage response consisting of a small immediate response followed by larger separate slower process. While that interpretation cannot be entirely ruled out, such ambiguity is inevitable given the experimental limitation of rapid but not instantaneous changes in stress. Keep in mind an additional difference between the shear stress response and those of fault normal displacement and *T*. For shear stress the transient is prolonged; Figure 14a shows the first 2 s of the much longer response, whereas fault normal displacement and transmitted amplitude have reached steady state in 2 s. So after 2 s shear stress is well short of its final target. Measuring the full shear stress response, the

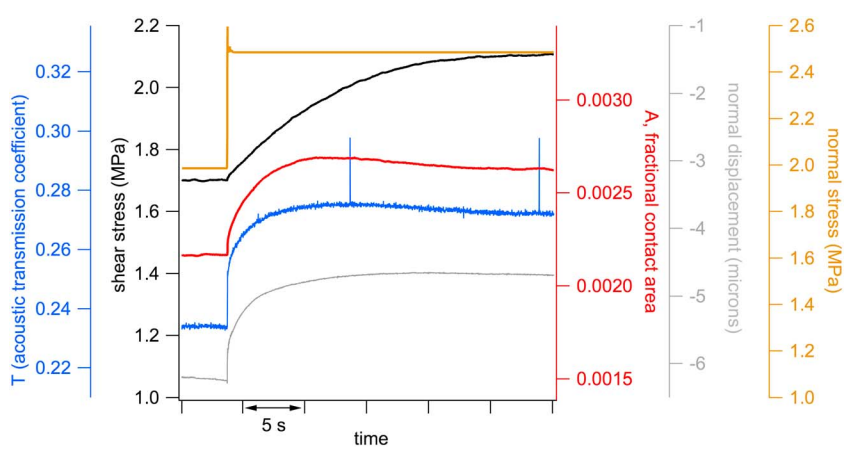

Figure 15. Relations among shear stress (black), fractional contact area (red), transmitted amplitude (blue), and fault normal displacement (gray) in response to a 25% step change in normal stress (yellow) from the published study on lucite friction [*Nagata et al.*, 2014].

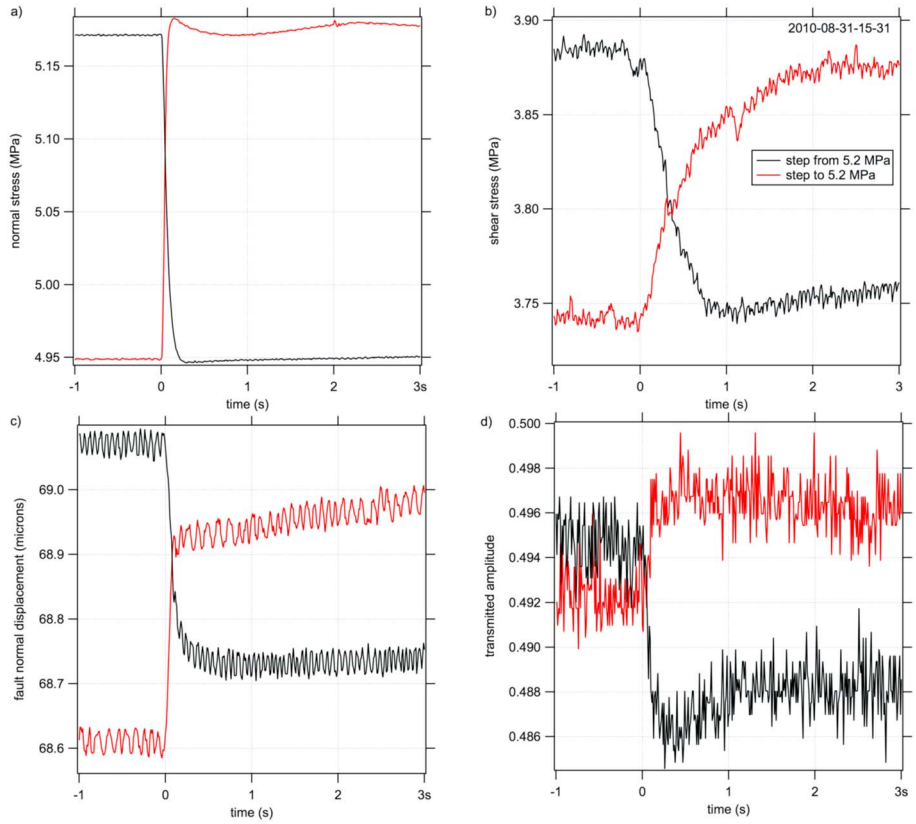

Figure 16. Detailed response of a step increase (red) and decrease (black) of 0.2 MPa. (a) Normal stress. In this case the step increase overshoots the target value and oscillates subsequently. In comparison to the typical step this is poorly controlled. The down step is better behaved with typically slight overshoot and well-controlled recovery. (b) Shear stress. Asymmetry in the response is probably influenced by nonconstant slip rate with a decrease in slip rate following normal stress increase and an increase in slip rate for normal stress decrease. (c) Fault normal displacement. (d) Transmitted amplitude.

transient is 91% of the total change in shear stress (Figure 14b). Despite there being a small amount of immediate change in shear stress, our favored interpretation is that shear strength follows a single-stage response and that the ~9% change that occurs during the normal stress increases is simply an artifact of the experimental technique in which normal stress changes are applied over a small but finite time. During that short time some slip and therefore some slip-dependent strength change occurs.

4.2.1. Relation to Contact Area

Experimental data that show the relations among shear stress, fault normal displacement, transmitted amplitude, and contact area during changes in normal stress are limited to exploratory experiments on the transparent analog material and lucite plastic (aka acrylic or PMMA) by *Nagata et al.* [2014]. Here their summary plot of the response of shear stress, normal displacement, transmitted amplitude [after *Nagata et al.*, 2012], and contact area [after *Dieterich and Kilgore*, 1994] for a 25% step in normal stress is reproduced as Figure 15. Whereas transmitted amplitude and normal displacement show a large immediate response, contact area shows a much smaller immediate response. Though these experiments indicate that during normal stress change transmitted amplitude and fault closure cannot be used directly as proxies for contact area, they suggest that a fault shear strength lags significantly behind nearly instantaneous changes in contact area resulting from changes in the applied normal stress to that fault. They also show that transmitted amplitude and fault normal displacement evolve over a similar slip length scale as contact area. Consistent with those lucite results, our step changes in normal stress on granite sliding at steady state result in changes normal displacement and transmitted amplitude that evolve over a similar length scale that is shorter than for shear resistance. Furthermore, in our granite experiments fault normal displacement and transmitted amplitude achieve steady state levels much more rapidly relative to shear resistance than for lucite. For these reasons, throughout the remainder of this paper we assume that the steady state normal displacement and

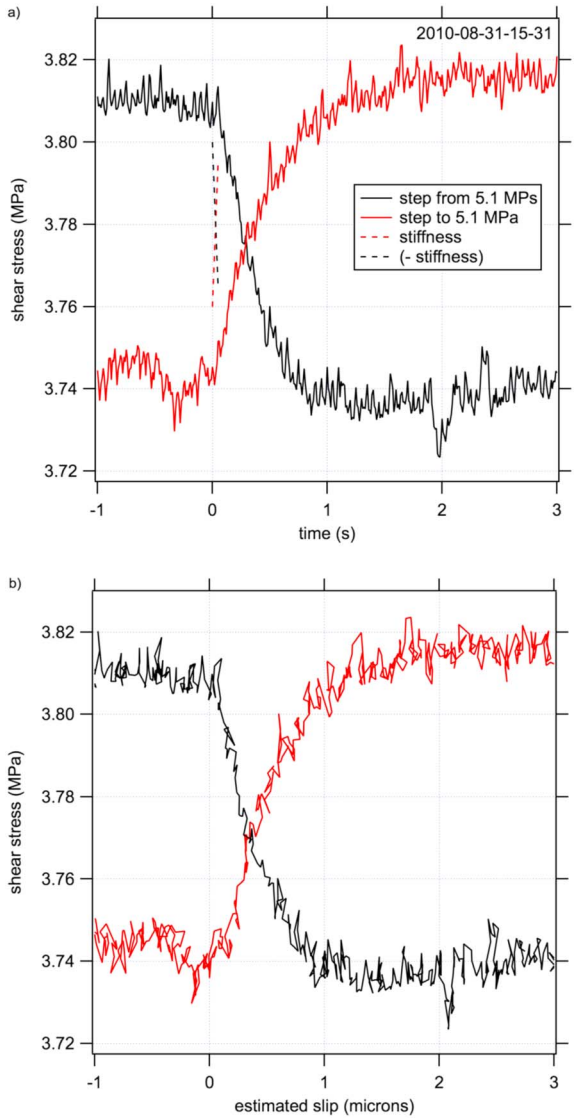

Figure 17. Detailed comparison of the symmetry of the response of shear stress to a normal step increase (red) and decrease (black) of 0.1 MPa. This is the smallest well-resolved step and, because of the small size, has the smallest excursions from the control load point velocity of 1 μm/s. (a) Time history. (b) Estimated slip history. Slip is calculated from the known stiffness, load point displacement, and the measured shear resistance (see text).

transmitted amplitudes can be used as a proxy for steady state contact area and that the slip necessary to reach those steady state is the same as required for contact area.

4.2.2. Shear Strength

This physical interpretation of the fault closure and transmitted amplitude data excludes a simple interpretation of shear strength, equation (5), because the inferred rapid changes in contact area are not accompanied by commensurate changes in shear resistance (Figure 16). In Figure 16 the evolution of shear resistance (b), fault normal displacement (c), and transmitted amplitude (d) are shown in response to changes in normal stress (a) at an expanded scale. These are the step increases and decreases for the smallest steps in which both shear resistance and transmitted amplitude are adequately resolved. This plot emphasizes the differences in the length scale of the evolution of normal displacement and transmitted amplitude and contrasts increases and decreases, acknowledging that there are larger slip speed excursions for the down steps. Similarly, and despite fault normal displacement and transmitted amplitude showing evidence consistent with a two stage physical model of contact area change, the gradual change in shear resistance independent of inferred contact area (Figures 3 and 16) does not require a two-stage model of strength such as advocated by *Linker and Dieterich* [1992] based on their two-stage shear resistance observations. At the same time, despite the evidence of a gradual change in strength, shear resistance changing over a different time or length scale as the contact area excludes *Prakash*'s [1998] explanation of a gradual, exponential change in contact area controlling the evolution of shear resistance in his experiments. So our observations are not fully consistent with either physical interpretation of the prior studies and also do not allow for a simple proportionality between shear resistance and contact area, equation (5).

There are two additional shear resistance observations that have implications for physical models of faulting and of these experiments. First, Figure 16b shows somewhat more rapid evolution of shear resistance with time for the step decreases in normal stress than for the increases. Likely this is mostly due to slip rate increasing during the down step and decreasing during the up step (see below). Figure 17 shows the smallest steps for which the shear resistance is well resolved (0.1 MPa steps). These are much more symmetric in time

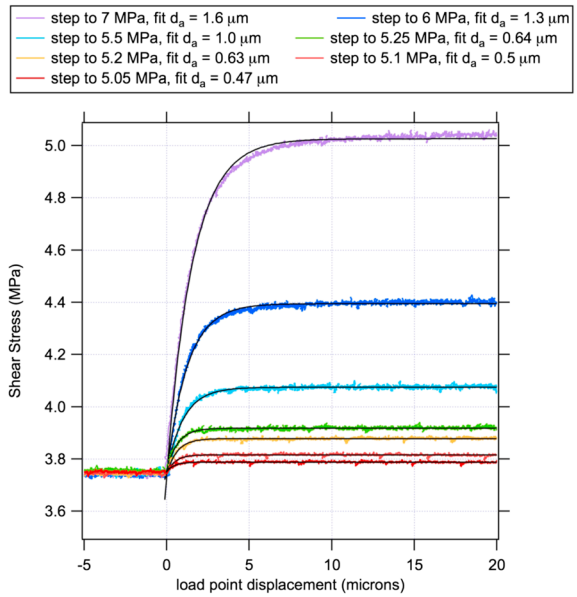

Figure 18. Complete form of shear stress response to increased normal stress. Fits to an exponential are shown with black lines. Fit parameters are listed in Table 1.

(Figure 17a), and here we have estimated fault slip δ from the controlled load point displacement d_L, the measured shear resistance, and known stiffness (k = 0.75 MPa/μm), $\delta = \delta_L - \frac{\tau}{k}$ (Figure 17b). There is an inperceptable difference in the horizontal axis between Figures 17a and 17b and any changes in slip speed associated with these small steps are unresolved by our measurements. Because of the apparent symmetry, the more extensive interpretable step increase data might be used to develop models of the response that are appropriate for either sense of stress change. In the following analysis we explore this idea in more detail using the entire range of stable steps.

Figure 18 shows the same data for shear stress from the step increases (Figure 3) at a longer horizontal scale of measured load point displacement, along with fits to each data set with a exponential function $\Delta\tau = \mu\Delta\sigma(1 - \exp(-\delta_L/d_a))$, where d_a is the apparent characteristic length, $\Delta\sigma$ is the imposed normal stress change, and μ is the steady state friction coefficient. The fit values of the product $\mu\Delta\sigma$ and d_a are listed in Table 1. The apparent length scale of the exponential d_a increases gradually with the size of the step (Table 1), while the form of the fit remains consistent with an exponential over the entire range of step sizes. As suggested for Figure 17, the increase in apparent length scale likely results primarily from a reduction in slip speed due the properties of the machine and the fault strength change that increases with the size of the normal stress step. To account for this and to compare the response of different sizes, we follow a normalization scheme developed by *Bhattacharya et al.* [2016] in which the shear stress change is normalized by the steady state change, such that the normalized amplitude is 1 for all steps. Then slip is calculated as above from load point displacement, shear stress, and stiffness (e.g., Figure 17b). The resulting normalized shear stresses versus estimated slip is shown in Figure 19a for the step increases, here superimposed ascending from small to large step (lowest signal to noise to highest) so that differences in the form of the smallest (red) and largest steps (purple) are visible. Most of the 3 times differences in apparent length are removed; however, the larger steps still have somewhat larger weakening distance. This may reflect an increase in the average contact dimension with normal stress, but for simplicity we ignore this difference and assume that the length scale does not dependent explicitly on normal stress.

Table 1. Fits to Normal Stress Steps (Figures 18 and 19) With an Exponential Function of Load Point Displacement

$\Delta\sigma$ (Nominal) MPa	$\mu\Delta\sigma$ MPa	d_a Microns	Figure
+0.05	0.036	0.47	18
+0.1	0.071	0.5	18
+0.2	0.14	0.63	18
+0.25	0.16	0.64	18
+0.5	0.32	1.0	18
+1	0.65	1.3	18
+2	1.28	1.6	18
− normalized	1	0.41	19d
+ normalized	1	0.55	19c

The same procedure was used on the well-behaved step decreases in normal stress $\Delta\sigma$ = −0.05, −0.1, −0.2, and −0.25 MPa (Figure 19b). The largest of these show a "hitch" or "ring" in the response thought to be due to slip acceleration and deceleration as the servo system responds to rapid slip and regains steady control of the load point displacement rate. This may be interpreted evidence of an intrinsic rate dependence of the fault. Nonethess the evolution distance for

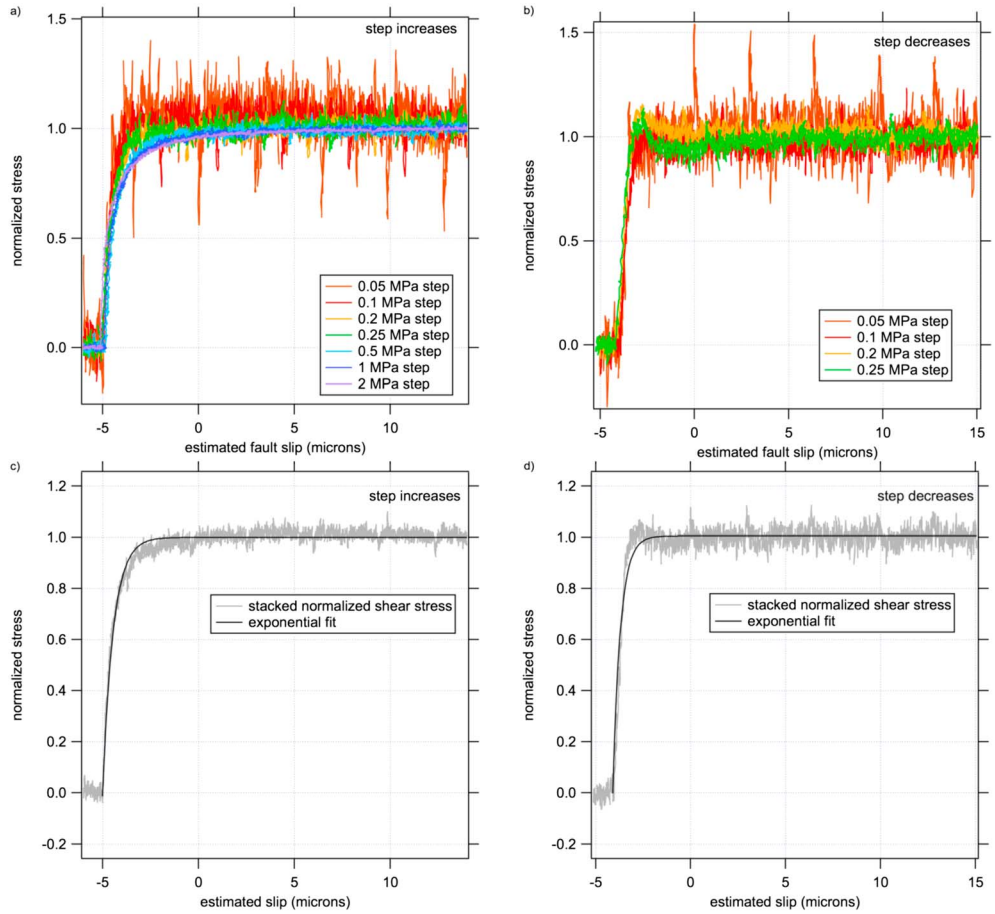

Figure 19. Characterized response to step changes in normal stress, after *Bhattacharya et al.* [2016]. Shear stress has been normalized by the steady state change in shear stress, such that the amplitude is 1 for all steps, and slip has been estimated from load point displacement and shear stress (see text). (a) Step increases from Figure 3, superimposed by ascending step size so that the highest signal to noise step (largest step) is on top. Color scheme as in Figure 3. (b) Same as Figure 19a but for step decreases. The two unstable steps from 6 and 7 MPa are excluded along with the nearly unstable step from 5.5 MPa (see Figure 5). (c) Stacked normalized shear stress from step increases (Figure 19a) to determine the average response. The black line is a fit to an exponential with d_c = 0.55 μm. (d) Same as Figure 19c but for step decreases (Figure 19c) and for step decreases (Figure 19b). d_c from the fit is 0.41 μm.

these small steps is very similar to the small up steps (Figure 19a, red). Figures 19c and 19d are the same data in parts Figures 19a and 19b, respectively, stacked and fit with an exponential function of slip. The characteristic slip distances are 0.55 μm and 0.41 μm for the up and down steps, respectively (Table 1). Given the control issues in these experiments, and the small step symmetry (Figure 17), in remainder of this report for the purposes of discussion, conceptual and actual modeling, we take these values to be the same.

4.3. Models of Shear Strength Evolution

To develop a plausible physical model of the collective step test data set, we use the four fundamental constraints from the observations: (1) steady state shear resistance is proportional to the real area of contact, i.e., equation (5) (as determined by the normal stress); (2) contact area follows a two-stage response to normal stress reaching steady state rapidly relative to shear strength; (3) shear strength changes gradually with displacement following a change in normal stress; and (4) that the characteristic length of the shear stress change is independent of the sign of the normal stress change.

Constraint (1) and the range of normal stress step sizes in these experiments require a somewhat different approach than in standard studies of rock friction [e.g., *Dieterich*, 1979; *Ruina*, 1983] that focus on second-

order dependencies on slip rate. Our study involves first-order stress changes and thus from (1) requires first-order changes in contact area. A qualitative two-stage response function for normal stress-dependent contact area that satisfies constraints (1) and (2) is detailed in Appendix A. The observations (2) and (3) require that shear stress shows a delayed response to changes in contact area, and our favored model that satisfies (1)–(3) is that shear resistance evolves following contact area exponentially in slip. Specifically, taking fractional contact area of a nominally flat but rough surface, the ratio of contact area A_c to total area A_t, $A = A_c/A_t$, to satisfy constraint (1), use the *Dieterich and Kilgore* [1994, 1996] observation that contact area is limited by the material yield stress, σ_y, and define a steady state fractional contact area.

$$A^{ss} = \frac{\sigma_n}{\sigma_c}, \tag{6a}$$

where σ_c is the contact-scale normal stress which is on the order of the material yield stress [e.g., *Beeler et al.*, 2016]. Yield stresses at room temperature are on the order of tens of gigapascals for crystalline rocks [e.g., *Dieterich and Kilgore*, 1996]. Equivalently and more generally, using a value of fractional contact area A_0 associated with a reference normal stress σ_0, (6a) can be expressed as

$$\frac{A^{ss}}{A_0} = \frac{\sigma_n}{\sigma_0}. \tag{6b}$$

To satisfy constraints (3) and (4), we borrow an idea from *Ruina* [1983] and take the shear resistance, s, to evolve with contact area, using the general form of (6a) and (6b), $\sigma_0\, A/A_0$, so that s follows area exponentially in slip using the standard "slip law" form of *Ruina* [1983]. With this form, s, can be thought of as being weighted memory of prior fractional contact area:

$$\frac{\mathrm{d}s}{\mathrm{d}t} = -\frac{V}{d_c}\left(s - \mu\sigma_0\frac{A}{A_0}\right), \tag{7a}$$

where μ is the friction coefficient and d_c is the characteristic contact dimension. Throughout our application of (7a), we assume that d_c is independent of normal stress, e.g., as might be inferred from *Greenwood and Williamson* [1966]. Since most of the inferred area change is more rapid with displacement than for shear stress (Figure 6) for simplicity take $A/A_0 \approx \sigma_n/\sigma_0$ at all times. Then (7a) depends on normal stress exponentially in slip, as required by the observations:

$$\frac{\mathrm{d}s}{\mathrm{d}t} = -\frac{V}{d_c}(s - \mu\sigma_n). \tag{7b}$$

Equation (7b) is the form used by *Prakash* [1998] to characterize the changes in shear resistance with normal stress during shock loading.

4.3.1. Simulated Response to Step Increases

In keeping with the first-order step sizes, to simulate step increases with (7b), we ignore standard second-order rate and state effects and assume that friction is constant. In the experiments the normal stress changes are not perfectly abrupt, so we represent the change in normal stress as an exponential function

$$\sigma = \sigma_0 + \Delta\sigma\left[1 - \exp\left(\frac{-(t - t_0)}{t_c}\right)\right], \tag{8}$$

where t_0 is the time the normal stress change $\Delta\sigma$ is initiated, σ_0 is the initial normal stress, and t_c is the characteristic duration of the change. In these calculations detailed in Appendix B, $t_c = 0.02$ s, which matches the duration of the imposed changes well [*Kilgore et al.*, 2012]. Keep in mind that t_c in these simulations was chosen qualitatively and somewhat arbitrarily. It is not a property of the fault but rather of the normal stress control system of the apparatus; nevertheless, large values of t_c tend to influence the detailed shear stress

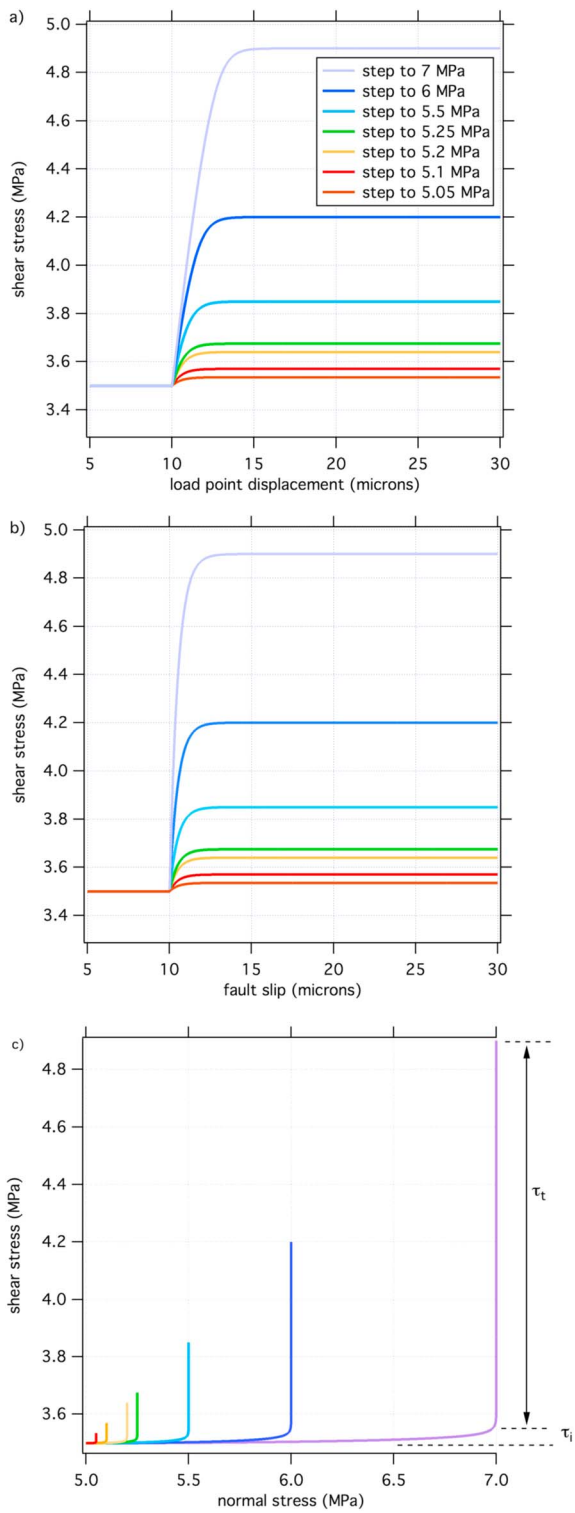

Figure 20. Slider block simulations of step increases with equations (7a), (7b), and (8) with μ = 0.7, d_c = 0.5 μm, k = 0.75 MPa/μm, and t_c = 0.02 s. (a) Shear stress versus load point displacement. (b) Shear stress versus fault slip. (c) Shear stress versus normal stress.

response. We use a slider block model to relate shear stress to slip, $\tau = k(\delta_L - \delta)$, and we equate shear stress on the fault to the fault strength that is defined by (7b). Figure 20 shows simulations with μ = 0.7 and d_c = 0.5 μm. These adequately capture the increase in apparent slip distance with step size (compare Figures 20a and 19b) but are not identical to the observations (Figure 18). Similarly, the simulations also produce a relatively small amount of apparent evolution of shear resistance during the stress step (compare Figure 20c with 14a). It appears from the comparison with the data that the duration of normal stress increase in the simulation is a bit shorter than in the actual experiments. In addition, matching the specific form of the observed change of shear stress with time, or loading displacement likely depends on the slip rate dependence and other fault property dependencies not included in (7b), the details of which are not well established [e.g., *Ruina*, 1980; *Bhattacharya et al.*, 2015].

5. Tests of the Inferred Response

Because these experiments of *Kilgore et al.* [2012] repeat those of *Linker and Dieterich* [1992], implicit in our interpretation is there is no difference between the intrinsic fault response in the two studies; in other words, our improved experimental technique and recordings revealed the response that was unresolved in the earlier study. To simultaneously explore this possibility in detail and to test the simple model response in equations (7a) and (7b), we examine the predictions for the two other types of tests in our complete data set: the pulse tests (Figure 7) and the stability of slip in response to step decreases in normal stress (Figure 8).

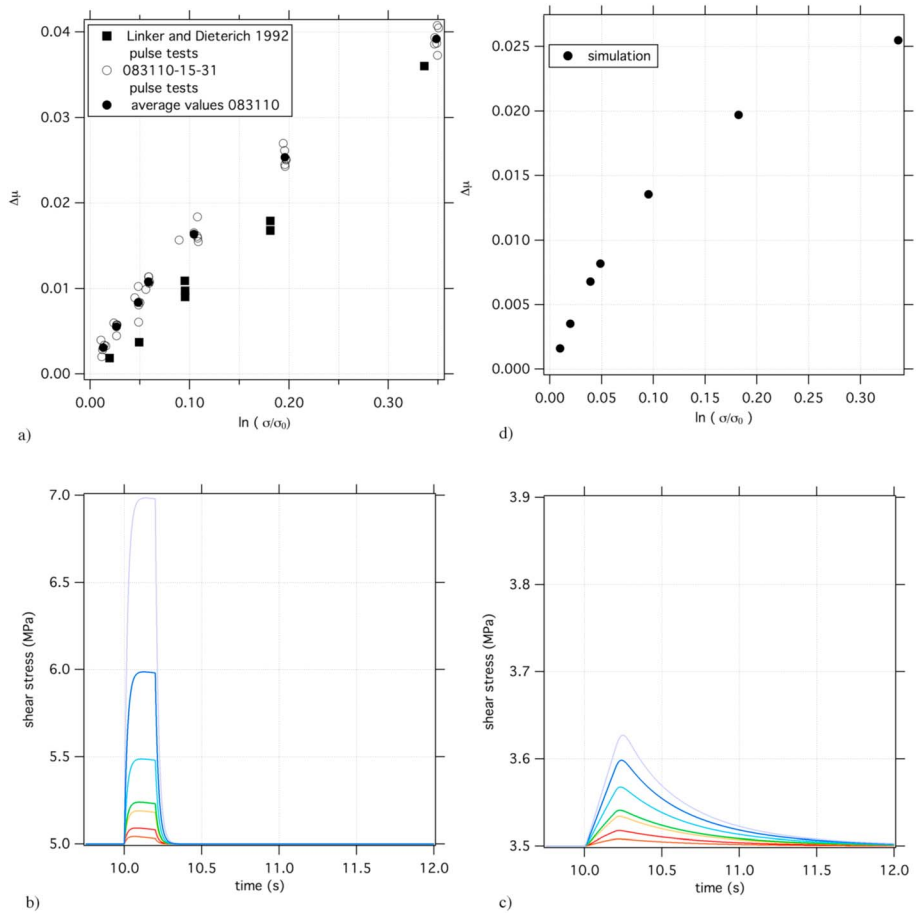

Figure 21. Pulse test summary. (a) The peak stresses from six sets of pulse tests (open symbols), each with seven amplitudes (0.05, 0.1, 0.2, 0.25, 0.5, 1, and 2 MPa) shown with their averages (solid circles) versus the natural logarithm of the ratio of the target normal stress to the starting value. Shown for comparison are the analogous measurements from *Linker and Dieterich* [1992]. (b and c) Slider block simulations of pulse tests with equation (7b) with $\mu = 0.7$, $d_c = 0.5$ μm, $k = 0.75$ MPa/μm, and a pulse duration of $\Delta t = 0.2$ s. (d) Summary of the pulse test simulations in Figure 21c plotted in the same format as Figure 21a.

5.1. Pulse Tests

The first comparison is between the pulse tests (Figure 7) and those of *Linker and Dieterich* [1992]. The test metric in Linker and Dieterich's data reduction is the eventual peak stress that follows their first and second response stages. Ideally, this peak would be unambiguous and well resolved in both studies, as opposed to being overprinted by coupling of normal stress to shear as in the Linker and Dieterich step tests. Unfortunately, there is at least some coupling of shear stress to normal stress in our pulse tests that is absent from the step tests. For instance, in Figure 7b, for the largest pulse amplitude the shear stress increases essentially immediately as the normal stress increases, and decreases immediately when the normal stress is reduced at the end of the pulse. The slope of these changes in shear stress versus time exceeds the stressing rate, k^*V_L, so there are machine effects, smaller but similar to those seen in *Linker and Dieterich* [1992]. This introduces ambiguity in the values of the peak stress. Whereas *Linker and Dieterich* [1992] always saw the immediate normal stress to shear stress coupling effect, regardless of pulse size, and used the analogous peak of the shoulder as the peak fault strength, since the coupling in our smaller steps is not large enough to produce a shoulder, we cannot remove the coupling from our pulse measurements. For internal consistency we use the overall peak stress from each of our pulse tests as our peak strength metric. Thus, our pulse test measurements cannot be directly equated with those from the earlier study. Not surprisingly, the peak strengths from pulse tests versus the natural logarithm of the ratio of target normal stress to the starting value (Figure 21a) differ in two ways to those in *Linker and Dieterich* [1992]; the 1992 data have lower

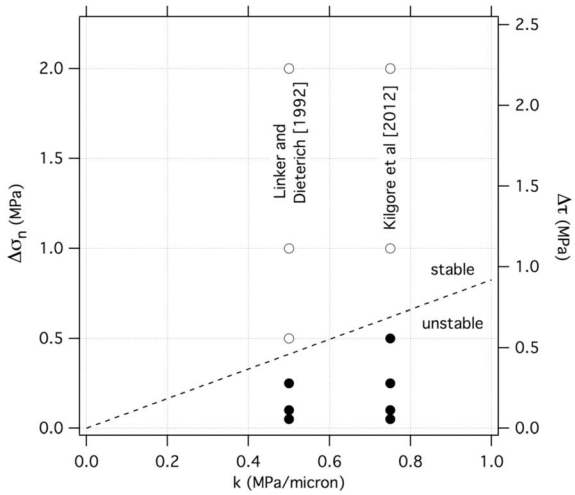

Figure 22. Approximate location of the boundary between stable and unstable response of slip to step decreases in normal stress (right axis) for the experiments of *Linker and Dieterich* [1992], k = 0.5 MPa/μm and *Kilgore et al.* [2012], k = 0.75 MPa/μm. Open and solid symbols denote unstable and stable responses, respectively. The dashed line is the estimated position of the boundary with a slope of 0.825 μm. The right axis is the measured steady state size of the shear stress change corresponding to step normal increases of the left axis (see Figure 6a).

values and are linear in log stress. Simulations with (7b) capture the nonlinearity of the peaks in our study (Figure 21d), but the simulated values are significantly smaller than actually observed in Figure 21a. While this may be due to coupling, this test neither confirms similarity between the two studies nor allows a self-consistent extrapolation of step results to the pulse tests. These remain open questions to be addressed in subsequent studies.

5.2. Stability

In laboratory experiments the stability of fault slip in response to increases in loading rate and decreases in normal stress depends on the stiffness of the fault, the rate fault strength changes with slip, and on the stiffness of loading system; the rate shear stress applied to the fault changes with displacement of the loading point [*Dieterich*, 1978]. Instability results when fault stiffness exceeds the loading stiffness, i.e., when the fault is able to lose strength more rapidly with displacement than the loading system displacement rate of stress change. For determining the effective stiffness of the fault, a useful technical advance of *Kilgore et al.* [2012] was to reduce the distance between the mounts of the fault slip sensor from the approximately ~30 mm of *Linker and Dieterich* [1992] to ~11 mm. This reduction stiffened the control system from ~0.5 MPa/μm to ~0.75 MPa/μm. The improved stability requires that the boundary in these two studies occurs at slightly different step amplitudes (Figure 22). The modest stability difference can be used with the empirical relation (7b) to characterize the fault properties, as follows. If we assume that the response of shear resistance to normal stress at constant slip rate is the simple exponential form, $\Delta\tau = \mu\Delta\sigma_n \exp\left(-\frac{\delta}{d_c}\right)$ from (7b), the maximum rate of slip weakening is $-\mu\Delta\sigma_n/d_c$. This is the critical stiffness of (7b), and the associated fault stability boundary in Figure 22 is

$$\Delta\sigma_n = \frac{d_c}{\mu} k_c. \tag{9}$$

For these experiments μ = 0.63 (Figure 9) and the boundary in Figure 22, with slope of 0.83 μm, corresponds to d_c = 0.52 μm. This is well within the range of weakening distances inferred empirically from the step tests. In other words, our assumption of consistency between the strength in response to stable step increases and decreases is verified by the position of the stability boundary. An important caveat is that we have ignored any rate dependence of the fault.

6. Discussion

The normal stress stepping experiments reported here and in the prior study [*Kilgore et al.*, 2012] resolve the inconsistency between the previously published experiments [*Linker and Dieterich*, 1992; *Prakash*, 1998] by determining that shear stress evolves smoothly and approximately exponentially with slip of the interface rather than following a two-stage response to normal stress change. That the fault strength may evolve purely with slip eliminates the problem discovered by *Rice et al.* [2001] and *Ranjith and Rice* [2001] that in

dimensioned calculations immediate changes in shear resistance accompanying a normal stress change are unstable and have no solution. However, it is surprising that rate-independent equations, (7b) and (9), well describe shear resistance and stability of slip in these experiments. Most prior work has shown that rate dependence is the most important friction property [*Dieterich*, 1979; *Ruina*, 1983]. Ideally, this type of normal stress dependence should be integrated into rate- and state-dependent friction models [e.g., *Prakash*, 1998], but at present it is unknown how to do that. For example, the experiments show that large changes in stress result in changes in the shear strength of the interface over the characteristic length scale, d_c, that is consistent with contact dimensions. Typically, that scale is attributed to a state variable which in rate and state friction models is only a second-order contribution to fault strength. Thus, a recasting of frictional constitutive equations to account for first-order changes in stress will have to include evolution of the first-order properties of the interface with slip (e.g., (7b)), as done in this context by *Prakash* [1998].

However, while *Prakash* [1998] proposed that shear resistance is the product of a rate- and state-dependent friction relation and a separate state variable with a contact dimension length scale that characterizes the normal stress dependence of the shear resistance (of the form of equation (7b)), there are fundamental problems with this approach. First, as mentioned earlier, the normal stress-dependent state variable represented fractional contact area in *Prakash* [1998] and our measurements are not consistent with that simple interpretation. Second, rate- and state-dependent friction as originally intended [*Dieterich*, 1978, 1979] already accounts for fractional contact area in determining shear resistance, as follows. Based on earlier work of *Bowden and Tabor* [1950, and others], *Dieterich* [1978, 1979] adopted the conceptual model (5) as a basis for rate and state friction, namely, that the shear resistance is the product of fractional contact area and an intrinsic shear resistance of the population of contacts on the interface, S,

$$\tau = SA. \tag{10}$$

By including in S a second-order direct positive dependence on slip rate ($S_0 + f(V)$) and in A a second-order gradually realized negative dependence on slip rate ($A_0 - g(V)$) while ignoring the product of second-order terms results in the basic form of RS friction ($\tau = \tau_0 + a\ln(V/V_0) + b\psi$) [*Dieterich*, 1979; *Ruina*, 1983]. Accordingly, the "direct effect" $a$lnV term results from the small dependence of S on slip rate and the "evolution effect" or state variable term ($b\psi$) from the small dependence of contact area on slip rate. In our experiments since shear resistance apparently does not strictly track contact area, this product representation needs to be rethought and modified. And there are some accounting issues with contact area that need to be addressed in a recasting of the *Prakash* [1998] normal stress formulation so that rate, state, and normal stress dependencies are internally consistent.

To that end, while our earlier suggestion that shear resistance evolves with contact area (equation (7a)) ensures that (5) or (10) is satisfied for steady state conditions, and as required by a shear force balance, it is hard to understand physically how fault strength such as represented by (7b) can remain nearly constant as contact area changes rapidly, particularly for a decrease in contact area. One possible way out of this apparent inconsistency is to first acknowledge that the strength of a fault cannot be measured without active slip. Therefore, rapid changes in fault properties, say, in contact area, that affect fault strength may not be quite so immediately temporally apparent in a shear resistance time series. Second, strength loss according to (7b) is most rapid immediately following a stress step. That is, according to (7b) the highest rate of strength loss associated with an instantaneous normal stress reduction is the immediate rate of slip weakening $\Delta\sigma_n\mu/d_c$. Some details of expected immediate effects are detailed in Appendix B (Figure B1) and verified in the slip-time histories of the normal stress step increases (Figure 23). Here as in the simulations with (7b) (Figure B1), the largest excursions from constant slip rate (constant slope in this plot of slip versus time) and the lowest slip rates coincide with the step. Thus, (7b) is a model where fault strength cannot change instantaneously in time and yet at high resolution still appears to produce immediate changes in strength.

Unfortunately, because the size of the slip rate change depends on the properties of the machine (stiffness) as well as on the imposed change in normal stress, some careful well-instrumented experiments in which the machine response can be accounted for, and of which there are thoughtful analyses, are needed to better and fully understand fault "strength" in this context. Such careful, well-instrumented, and interpretable

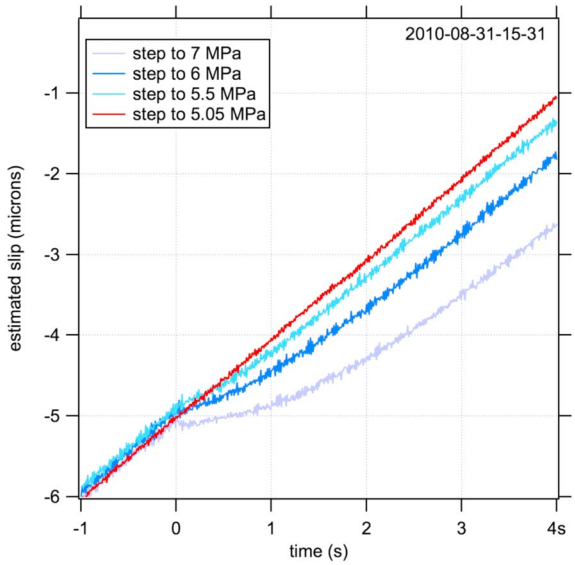

Figure 23. Observed excursions in slip with time due to apparently immediate changes in fault strength associated with normal stress increases. The normal stress change denoted in the legend is imposed at time equal zero.

experiments would be more easily conducted in a geometry other than DDS. Corrections of fault normal strain due to coupling to shear and normal stress is unique to this geometry and do not arise, for example, in rotary shear [*Bhattacharya et al.*, 2016]. Similarly, the strong tendency to observe coupling between normal stress and shear stress (e.g., *Linker and Dieterich* [1992] and *Hong and Marone* [2005], and in the pulse tests in this study (Figure 7b)) is a consequence of the relative orientation of the applied stresses in DDS, is difficult to avoid, and is absent in other standard configurations. Moreover, and related to these issues is the presence of two faults (Figure 2) which may have slightly different properties in response to the rapidly applied stress changes, or which may see slightly different stress changes due to small misalignment of the loading frames, small deviations of the side block fault surfaces to perfectly parallel to the normally loaded side block surfaces, deviations from the two center block fault surfaces from being perfectly parallel, from the shear loaded surface of the center block from being perpendicular to the applied shear load, or from that surface from being perfectly perpendicular to both of the faults. Again, these are issues unique to DDS. In the case of our experiments, only one of the faults is instrumented and while much might be gained by separately measuring displacements across both faults, many potential and real problems would be avoided by using a geometry with a single fault.

That said, these normal stress change experiments have proven difficult to interpret even given high-quality measurements that lack stress coupling machine effects (Figures 3 and 8), and while a strong motivation for experimentalists is to minimize the influence of the apparatus, there are two additional issues to keep in mind before going to extreme lengths to conduct room temperature experiments that improve upon those in this report. First are the issues of the changes in slip rate that invariably result when normal stress is changed (Figures 22 and B1), independent of the fault's intrinsic rate dependence. Since these depend on the loading system stiffness [*Shimamoto et al.*, 1980; *Kilgore et al.*, 2017], all of those have to be well characterized in independent tests. Obviously, these effects will depend on the machine of choice, making comparisons between studies more difficult. Second, as pointed out by *Nagata et al.* [2014] in a different but related context, improvements in experimental technique should produce a clearer understanding of the relationship between normal stress change and shear resistance in dry room temperature experiments. Establishing the contact scale physics that controls shear resistance at room temperature would be a significant first step to understanding the range of natural temperatures and stresses over which the response represented by equation (7b) will apply. However, the cases of interest to natural fault mechanics are for rocks at higher normal stresses, undergoing localized slip within saturated shear zones at elevated temperature and in the presence of reactive fluids. Determining whether or not the empirical relation (7b) can be applied under such conditions may be of greater practical need than a deeper understanding of the contact scale micromechanics of dry room temperature rock friction.

7. Summary

In room temperature dry friction experiments on initial bare rock surfaces of granite at normal stresses between 5 and 7 MPa, rapid normal stress changes result in gradual, approximately exponential changes in shear resistance with fault slip. The characteristic distance of the shear resistance evolution is on the

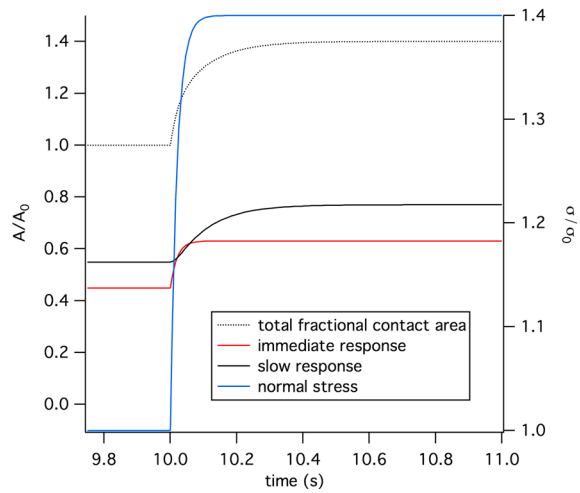

Figure A1. Simulated change in fractional contact area (left axis) for a 40% change in fractional normal stress (right axis) using equation (A1c) in Appendix A.

order of 0.5 μm. In contrast, fault normal displacement and the amplitude of small high-frequency elastic waves transmitted across the surface follow a two-stage response to rapid normal stress changes: a large immediate and a smaller gradual response with slip. The gradual response has a similar slip distance for normal displacement and transmitted amplitude; however, it is significantly smaller than that of shear resistance. Based on a prior study that showed the same characteristic distance for contact area, transmitted amplitude, and fault normal displacement, we infer that shear resistance following normal stress changes does not directly or immediately track changes in contact area on the fault.

The shear resistance has a similar characteristic length for both increases and decreases in normal stress, at least for the smallest stress changes that are not highly affected by slip speed excursions associated with the step change. Furthermore, the stability of sliding in response to large step decreases in normal stress is well predicted using the slip length observed in step increases. Analysis of the shear resistance and slip time histories suggests that nearly immediate changes in strength occur in response to rapid changes in normal stress; these are manifested as a change in slip speed immediately at the step change in normal stress, despite the gradual change in measured shear stress. These changes in slip speed can be accounted for in models using rate-independent strength. Our interpretation is that the size of this acceleration or deceleration response depends on fault properties, the size of the stress change and the characteristics of the testing machine.

Appendix A: Two-Stage Representation of Closure, Transmitted Amplitude, or Contact Area Change

Following *Linker and Dieterich* [1992], here we present a two-stage model that might be used to represent closure, transmitted amplitude, or contact area in experiments with variable normal stress and slip speed. The approach is motivated by our observations (e.g., Figures 3–5) from step increases, the prior conceptual model of *Linker and Dieterich* [1992], and the many observations of low-temperature friction [e.g., *Dieterich*, 1978, 1979; *Ruina*, 1983] that indicate changes in strength associated with variable slip speed are small relative to the ambient strength. Accordingly, fractional contact area, closure, and transmitted amplitude depend on slip speed and normal stress and these dependences can be partitioned into two components, an immediate dependence on normal stress and a slower component that depends on normal stress and slip speed. Here our development uses fractional contact area A as an example:

$$A(\sigma_n, V) = A_i(\sigma_n) + A_t(\sigma_n, V) \tag{A1a}$$

The immediate dependence on normal stress can be parameterized defining an arbitrary reference normal stress σ_0 with associated fractional contact area A_0 and the immediate dependence is

$$\frac{1}{A_0}\frac{\mathrm{d}A_i}{\mathrm{d}t} = \frac{1}{\sigma_0}\frac{\mathrm{d}\sigma_n}{\mathrm{d}t}. \tag{A1b}$$

The slow response to normal stress here is somewhat arbitrarily represented by *Ruina*'s [1983] slip formulation

$$\frac{1}{A_0}\frac{\mathrm{d}A_t}{\mathrm{d}t} = -\frac{V}{d_t}\left(\frac{A_t}{A_0} - \frac{\sigma_n}{\sigma_0}\right) \tag{A1c}$$

where d_t is the characteristic slip distance and such that at steady state the slow contribution to fractional contact area is $A_t^{ss} = A_0\sigma_n/\sigma_0$. The choice also requires that the intrinsic response of fractional contact area to changes in normal stress is to evolve exponentially in slip. Figure A1 shows the behavior of equation (A1c) in response to changes in normal stress. In this example 45% of the response is immediate and the characteristic length is 0.1 μm.

Because steady state contact area is known also to depend on slip speed [e.g., *Dieterich and Kilgore*, 1994; *Nagata et al.*, 2014] (A1c) can be expanded to include a slip rate dependence,

$$\frac{1}{A_0}\frac{\mathrm{d}A_t}{\mathrm{d}t} = -\frac{V}{d_t}\left(\frac{A_t}{A_0} + \beta \ln\frac{V}{V_0} - \frac{\sigma_n}{\sigma_0}\right). \tag{A1d}$$

Here the value A_0 is that associated with sliding at the reference slip speed V_0 at the reference normal stress σ_0. Guidance on the magnitude of the β coefficient can be found in the prior studies of transparent materials [*Dieterich and Kilgore*, 1994, 1996; *Nagata et al.*, 2014]. Accordingly, for consistency with rate and state friction formulations, β is second order, typically between 1 and 2%. That is, when normal stress is at the reference stress, the steady state value $A^{ss}/A_0 = 1 + \beta \ln(V_0/V)$, with $0.01 \le \beta \le 0.02$.

Appendix B: Immediate Effects of Changing Normal Stress on Slip Speed

The effect of fault stress change on the rate of fault slip in a laboratory test depends on the elastic properties of the fault and testing machine, the size of the stress change, and on the particular sensitivity of the fault strength, s, to the change. These various contributions can be illustrated for quasi-static slip, where the fault strength and shear stress are equal, using a single degree of freedom slider block model

$$\frac{\mathrm{d}s}{\mathrm{d}\delta} = k\left(\frac{V_L}{V} - 1\right), \tag{B1a}$$

where V_L is the velocity of the load point of the testing machine and k is the stiffness. Rearranging to solve for the slip speed, V, is

$$V = \frac{V_L}{\frac{1}{k}\frac{\mathrm{d}s}{\mathrm{d}\delta} + 1}. \tag{B1b}$$

For a fault initially sliding at steady state at the loading rate, changes in slip speed associated with an imposed stress change depend on fault stiffness and on the rate fault strength changes with slip. Slip rate decreases if the fault strength goes up with displacement; the lower the stiffness the more pronounced the effect.

Using examples from *Kilgore et al.*'s [2012] step increases in normal stress as a guide and following explicit recommendations from USGS internal reviewer Path Bhattacharya, we show the influence of changing fault strength on slip speed for a system in which the fault has no rate dependence of strength, and immediate velocity excursions arise from gradual but nonetheless apparently rapid changes in fault strength. We take the evolution of fault strength following a change in normal stress to be the *Prakash* [1998]-like evolution

$$\frac{\mathrm{d}s}{\mathrm{d}\delta} = -\frac{(s - \mu_0\sigma_n)}{d_c}. \tag{B2}$$

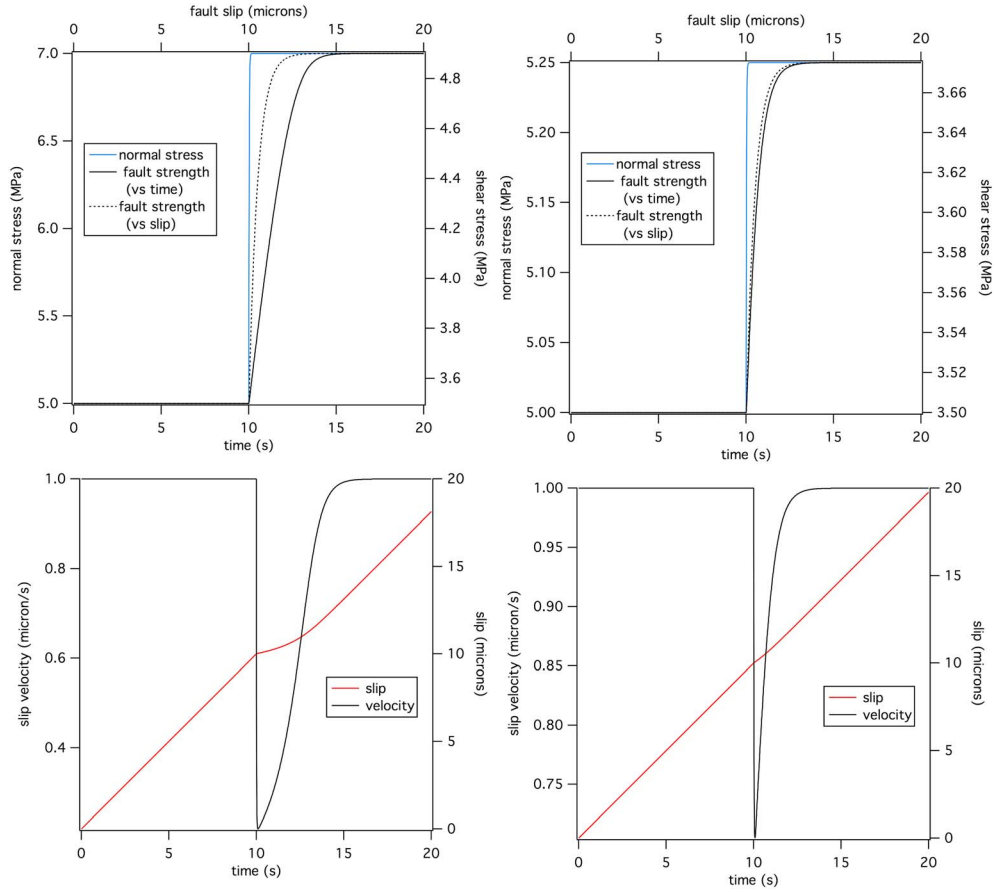

Figure B1. Simulated change in shear stress, shear strength, slip velocity, and slip with a change in normal stress using equations (B1a), (B1b), and (B2). (left column) The response to a 2 MPa change in normal stress with $\sigma_0 = 5$ MPa, $d_c = 0.5$ MPa, and $k = 0.75$ MPa/μm. (top row) Stress versus time (lower axis) and slip (upper axis). (bottom row) Slip velocity (left axis) and slip (right axis) versus time. (right column) The response to a 0.25 MPa change in normal stress using the same plots as in Figure B1 (left column).

Here d_c is a characteristic weakening distance, σ_n is normal stress, and μ_0 is a constant friction coefficient. Combining with (B1a) results in the slip rate

$$V = \frac{V_L}{1 - \frac{(s - \mu_0 \sigma_n)}{k d_c}}. \tag{B3}$$

For a fault sliding at steady state at V_L, an instantaneous change in normal stress from an initial value σ_0 to final σ_f, produces shear strength (3) that is exponential in slip

$$s = \mu_0 \sigma_f - \mu_0 \Delta\sigma_n \exp\left(\frac{-\delta}{d_c}\right), \tag{B4a}$$

with a steady state value $\mu_0 \sigma_f$. For this case the slip velocity following the stress change has the analytical solution that results from substituting (B4a) for s and σ_f for σ_n in (B3),

$$V = \frac{V_L}{1 + \frac{\mu_0 \Delta\sigma_n}{k d_c} \exp\left(\frac{-\delta}{d_c}\right)}. \tag{B4b}$$

Accordingly, for an abrupt increase in normal stress, though the fault strength does not strictly change without slip and changes gradually at that, the slip speed immediately changes from V_L to $V_L/\left(1+\frac{\mu_0\Delta\sigma_n}{kd_c}\right)$. Thus, the change in slip speed depends on the size of the stress change ($\Delta\sigma_n$), the elastic properties of the loading system (k) and the fault properties (μ_0 and d_c).

In the *Kilgore et al.* [2012] experiments the normal stress changes are not so abrupt. To model these, we use the general forms of the slider block and fault strength, equations (B1a) and (B1b), and (B2), respectively. The simulations start from 5 MPa normal stress; rapid step changes in normal stress are imposed following $\sigma=\sigma_0+\Delta\sigma\left[1-\exp\left(\frac{-(t-t_0)}{t_c}\right)\right]$. Here t_0 is the time the normal stress change $\Delta\sigma$ is initiated, σ_0 is the initial normal stress, t_c is the characteristic duration of the normal stress change, and t_c = 0.02 s (this is a reasonable representation of the steps in the 2012 experiments). Loading velocity is 1 μm/s, d_c = 0.5 μm. For a step of 2 MPa normal stress (Figure B1, left column), there is a significant excursion in slip speed (lower plot). The recovery time is quite long. As a consequence there is an apparent lengthening of the time to get to steady state (top plot), despite this fault having no intrinsic rate dependence. For comparison is a much smaller step of 0.25 MPa (Figure B1, right column). In these *Kilgore et al.* [2012] experiments, the fault strength and machine interactions can explain the immediate reduction in slip speed associated with the normal stress increase (see Figure 23, in the text), and the lengthening of the apparent strength evolution distance (by ~3 times) as the step size increases, independent of the rate dependence of the fault itself. As for the abrupt stress changes, equation (5), the size of the slip speed excursions depend on loading system properties (k), fault properties (μ_0, d_c), and upon the size of the imposed change in stress ($\Delta\sigma_n$).

Acknowledgments
All original source data used in the figures and analysis in this report are publically available from the USGS repository: https://www.sciencebase.gov/catalog/item/595d37f0e4b0d1f9-f055aa26 or from the corresponding author (N.M.B.). The preliminary experimental observations that led to our extended study of normal stress effects were conducted by Kohei Nagata of the Earthquake Research Institute with BK at USGS during a USGS Venture Capital sponsored study with Masao Nakatani of the ERI. Many thanks to Kohei and Masao for their significant contributions to our understanding of rock friction. This research was supported by the Southern California Earthquake Center (contribution 7237). SCEC is funded by NSF Cooperative Agreement EAR-1033462 and USGS Cooperative Agreement G12AC20038. Conversations over a number of years with collaborators Path Bhattacharya and Allan Rubin, and mentor Jim Dieterich, are gratefully acknowledged. Path, Michael Barall, Brett Carpenter, and Francois Passelegue provided USGS and JGR reviews that significantly improved this paper. During review Path provided the solution upon which our Appendix B is based. Any use of trade, firm, or product names is for descriptive purposes only and does not imply endorsement by the U.S. Government.

References

Andrews, D. J., and Y. Ben-Zion (1997), Wrinkle-like slip pulse on a fault between different materials, *J. Geophys. Res.*, *102*(1), 552–571, doi:10.1029/96JB02856.

Balik, J.-M. R. B., and Thompson (1984), Ultrasonic scattering from imperfect interfaces: A quasi-static model, *J. Nondestruct. Eval.*, *4*, 177–196, doi:10.1007/BF00566223.

Beeler, N. M., and S. H. Hickman (2001), A note on contact stress and closure in rock joint and fault models, *Geophys. Res. Lett.*, *28*, 607–610, doi:10.1029/2000GL011458.

Beeler, N. M., G. Hirth, A. Thomas, and R. Bürgmann (2016), Effective stress, friction, and deep crustal faulting, *J. Geophys. Res. Solid Earth*, *121*, 1040–1059, doi:10.1002/2015JB012115.

Bhat, H. S., R. Dmowska, J. R. Rice, and N. Kame (2004), Dynamic slip transfer from the Denali to Totschunda Faults, Alaska: Testing theory for fault branching, *Bull. Seismol. Soc. Am.*, *94*, S202-S213, doi:10.1785/0120040601.

Bhattacharya, P., A. M. Rubin, E. Bayart, H. M. Savage, and C. Marone (2015), Critical evaluation of state evolution laws in rate and state friction: Fitting large velocity steps in simulated fault gouge with time-, slip-, and stress-dependent constitutive laws, *J. Geophys. Res. Solid Earth*, *120*, 6365–6385, doi:10.1002/2015JB012437.

Bhattacharya, P., A. M. Rubin, and T. E. Tullis (2016), Where did the time go? Friction evolves with slip following large velocity and normal stress steps, chap. 5 of PhD thesis, Princeton Uni., 28th Nov. [Available at http://arks.princeton.edu/ark:/88435/dsp01cr56n350m.]

Bouchon, M., and D. Streiff (1997), Propagation of a shear crack on a nonplanar fault: A method of calculation, *Bull. Seismol. Soc. Am.*, *87*(1), 61–66.

Bowden, F. P., and D. Tabor (1950), *The Friction and Lubrication of Solids*, 374 pp., Oxford Univ. Press. New York.

Brace, W. F., B. W. Paulding, and C. H. Scholz (1966), Dilatancy in the fracture of crystalline rock, *J. Geophys. Res.*, *71*, 3939–3953, doi:10.1029/JZ071i016p03939.

Brown, S. R., and C. H. Scholz (1985), The closure of random elastic surfaces in contact, *J. Geophys. Res.*, *90*, 5531–5545, doi:10.1029/JB090iB07p05531.

Dieterich, J. H. (1978), Time-dependent friction and the mechanics of stick slip, *Pure Appl. Geophys.*, *116*, 790–806, doi:10.1007/BF00876539.

Dieterich, J. H. (1979), Modeling of rock friction: 2. Simulation of preseismic slip, *J. Geophys. Res.*, *84*(B5), 2169–2175, doi:10.1029/JB084iB05p02169.

Dieterich, J. H. (2007), Applications of rate- and state-dependent friction to models of fault slip and earthquake occurrence, in *Treatise on Geophysics*, *Earthquake Seismol.*, vol. 4, edited by H. Kanamori, pp. 107–129, Elsevier, Boston, Mass.

Dieterich, J. H., and B. D. Kilgore (1994), Direct observation of frictional contacts: New insights for state-dependent properties, *Pure Appl. Geophys.*, *143*, 283–302, doi:10.1007/BF00874332.

Dieterich, J. H., and B. D. Kilgore (1996), Imaging surface contacts: Power law contact distributions and contact stresses in quartz, calcite, glass and acrylic plastic, *Tectonophysics*, *256*, 219–239, doi:10.1016/0040-1951(95)00165-4.

Dieterich, J. H., and M. F. Linker (1992), Fault stability under conditions of variable normal stress, *Geophys. Res. Lett.*, *19*(16), 1691–1694, doi:10.1029/92GL01821.

Duan, B., and D. D. Oglesby (2005), Multicycle dynamics of nonplanar strike-slip faults, *J. Geophys. Res.*, *110*, B03304, doi:10.1029/2004JB003298.

Escartin, J., G. Hirth, and B. Evans (1997), Nondilatant brittle deformation of serpentinites; implications for Mohr-Coulomb theory and the strength of faults, *J. Geophys. Res.*, *102*, 2897–2913, doi:10.1029/96JB02792.

Escartin, J., M. Andreani, G. Hirth, and B. Evans (2008), Relationships between the microstructural evolution and the rheology of talc at elevated pressures and temperatures, *Earth Planet. Sci. Lett.*, *268*, 463–475, doi:10.1016/j.epsl.2008.02.004.

Fang, Z., J. H. Dieterich, K. B. Richards-Dinger, and G. Xu (2011), Earthquake nucleation on faults with nonconstant normal stress, *J. Geophys. Res.*, *116*, B09307, doi:10.1029/2011JB008196.

Felzer, K. R., and E. E. Brodsky (2006), Decay of aftershock density with distance indicates triggering by dynamic stress, *Nature*, *441*, 735–738, doi:10.1038/nature04799.

Goodman, R. E. (1976), *Methods of Geological Engineering in Discontinuous Rocks*, 472 pp., West, New York.

Greenwood, J. A., and J. Williamson (1966), Contact of nominally flat surfaces, *Proc. R. Soc. London, Ser. A*, *295*, 300–319, doi:10.1098/rspa.1966.0242.

Hardebeck, J. L., and E. Hauksson (2001), Crustal stress field in Southern California and its implications for fault mechanics, *J. Geophys. Res.*, *106*, 21,859–21,882, doi:10.1029/2001JB000292.

Harris, R. A., and S. M. Day (1993), Dynamics of fault interaction-parallel strike-slip faults, *J. Geophys. Res.*, *98*(B3), 4461–4472, doi:10.1029/92JB02272.

Harris, R. A., and S. M. Day (1997), Effects of a low-velocity zone on a dynamic rupture, *Bull. Seismol. Soc. Am.*, *87*(5), 1267–1280.

Harris, R. A., and S. M. Day (2005), Material contrast does not predict earthquake rupture propagation direction, *Geophys. Res. Lett.*, *32*, L23301, doi:10.1029/2005GL023941.

Harris, R. A., R. J. Archuleta, and S. M. Day (1991), Fault steps and the dynamic rupture process—2-D numerical simulations of a spontaneously propagating shear fracture, *Geophys. Res. Lett.*, *18*(5), 893–896, doi:10.1029/91GL01061.

Hill, D. P. (2012), Dynamic stresses, Coulomb failure, and remote triggering-corrected, *Bull. Seismol. Soc. Am.*, *102*(6), 2313–2336, doi:10.1785/0120120085.

Hobbs, B. E., and B. H. G. Brady (1985), Normal stress changes and the constitutive law for rock friction (abstract), *Eos Trans. AGU*, *66*, 385.

Hong, T., and C. Marone (2005), Effects of normal stress perturbations on the frictional properties of simulated faults, *Geochem. Geophys. Geosyst.*, *6*, Q03012, doi:10.1029/2004GC000821.

Kame, N., J. R. Rice, and R. Dmowska (2003), Effects of pre-stress state and rupture velocity on dynamic fault branching, *J. Geophys. Res.*, *108*(B5), 2265, doi:10.1029/2002JB002189.

Kendall, K., and D. Tabor (1971), An ultrasonic study of the area of contact between stationary and sliding surfaces, *Proc. R. Soc. London, Ser. A*, *323*, 321–340, doi:10.1098/rspa.1971.0108.

Kilgore, B., J. Lozos, N. M. Beeler, and D. Oglesby (2012), Laboratory observations of fault strength in response to changes in normal stress, *J. Appl. Mech.*, *79(3)*, 031007–031007, doi:10.1115/1.4005883.

Kilgore, B., A. McGarr, N. M. Beeler, and D. A. Lockner (2017), Earthquake source properties from instrumented stick-slip, in *Fault Zone Dynamic Processes: Evolution of Fault Properties During Seismic Rupture*, *Geophys. Monogr. Ser.*, vol. 227, edited by M. Thomas, H. S. Bhat, and T. Mitchell, pp. 151–170, AGU and John Wiley, Washington, D. C., and Hoboken.

Linker, M. F., and J. H. Dieterich (1992), Effects of variable normal stress on rock friction: Observations and constitutive equations, *J. Geophys. Res.*, *97*, 4923–4940, doi:10.1029/92JB00017.

Lozos, J. C., D. D. Oglesby, B. Duan, and S. G. Wesnousky (2011), The effects of double fault bends on rupture propagation: A geometrical parameter study, *Bull. Seismol. Soc. Am.*, *101*(1), 385–398, doi:10.1785/0120100029.

Marone, C., and B. Kilgore (1993), Scaling of the critical slip distance for seismic faulting with shear strain in fault zones, *Nature*, *362*, 618–621.

Marone, C., C. B. Raleigh, and C. H. Scholz (1990), Frictional behavior and constitutive modeling of simulated fault gouge, *J. Geophys. Res.*, *95*, 7007–7025.

Martin, R. J. III, K. B. Coyner, and R. W. Haupf (1990), Physical properties measurements on analog granites related to the joint verification experiment, New England Research Report, GL-TR-90-0120 ADA230571.

Nagata, K., M. Nakatani, and S. Yoshida (2008), Monitoring frictional strength with acoustic wave transmission, *Geophys. Res. Lett.*, *35*, L06310, doi:10.1029/2007GL033146.

Nagata, K., M. Nakatani, and S. Yoshida (2012), A revised rate- and state-dependent friction law obtained by constraining constitutive and evolution laws separately with laboratory data, *J. Geophys. Res.*, *17*, B02314, doi:10.1029/2011JB008818.

Nagata, K., B. Kilgore, N. Beeler, and M. Nakatani (2014), High-frequency imaging of elastic contrast and contact area with implications for naturally observed changes in fault properties, *J. Geophys. Res. Solid Earth*, *119*, 5855–5875, doi:10.1002/2014JB011014.

Nakatani, M. (2001), Conceptual and physical clarification of rate and state friction: Frictional sliding as a thermally activated rheology, *J. Geophys. Res.*, *106*, 13,347–13,380, doi:10.1029/2000JB900453.

Oglesby, D. D. (2005), The dynamics of strike-slip step-overs with linking dip-slip faults, *Bull. Seismol. Soc. Am.*, *95*(5), 1604–1622, doi:10.1785/0120050058.

Olsson, W. A. (1988), The effects of normal stress history on rock friction, key questions in rock mechanics, in *Proceedings of the 29th U.S. Symposium*, edited by P. A. Cundall, R. L. Sterling, and A. M. Starfield, pp. 111–117, Univ. of Minnesota, Balkema.

Power, W. L., and T. E. Tullis (1992), The contact between opposing fault surfaces at Dixie Valley, Nevada, and implications for fault mechanics, *J. Geophys. Res.*, *97*, 15,425–15,435, doi:10.1029/92JB01059.

Prakash, V. (1998), Frictional response of sliding interfaces subjected to time varying normal pressures, *J. Tribol.*, *120*, 97–102, doi:10.1115/1.2834197.

Pyrak-Nolte, L. J., N. G. W. Cook, and L. R. Myer (1987), Seismic visibility of fractures, 28th US Symposium on Rock Mechanics, Tuscon, Arizona, June 29 – July 1, 1987.

Pyrak-Nolte, L. J., L. R. Myer, and N. G. W. Cook (1990), Transmission of seismic waves across single natural fractures, *J. Geophys. Res.*, *95*, 8617–8638, doi:10.1029/JB095iB06p08617.

Ranjith, K., and J. R. Rice (2001), Slip dynamics at an interface between dissimilar materials, *J. Mech. Phys. Solids*, *49*, 341–361, doi:10.1016/S0022-5096(00)00029-6.

Rice, J. R., N. Lapusta, and K. Ranjith (2001), Rate and state dependent friction and the stability of sliding between elastically deformable solids, *J. Mech. Phys. Solids*, *49*, 1865–1898, doi:10.1016/S0022-5096(01)00042-4.

Richards, P. G. (1976), Dynamic motions near an earthquake fault: A three-dimensional solution, *Bull. Seismol. Soc., Am.*, *66*, 1–32.

Richards-Dinger, K., R. S. Stein, and S. Toda (2010), Decay of aftershock density with distance does not indicate triggering by dynamic stress, *Nature*, *467*, 583–586, doi:10.1038/nature0940.

Ruina, A. L. (1980), Friction laws and instabilities, a quasistatic analysis of some dry frictional behavior, PhD thesis, 99 pp., Brown Univ.

Ruina, A. L. (1983), Slip instability and state variable friction laws, *J. Geophys. Res.*, *88*, 10,359–10,370, doi:10.1029/JB088iB12p10359.

Schoenberg, M. (1980), Elastic wave behavior across linear slip interfaces, *J. Acoust. Soc. Am.*, *68*, 1516–1521, doi:10.1121/1.385077.

Scholz, C. H., and J. T. Engelder (1976), The role of asperity indentation and ploughing in rock friction: I. Asperity creep and stick-slip, *Int. J. Rock Mech. Sci. Geomech. Abstr.*, *13*, 149–154.

Shimamoto, T., J. Handin, and J. M. Logan (1980), Specimen-apparatus interaction during stick-slip in a triaxial compression machine: A decoupled tow-degree of freedom model, *Tectonophysics*, *67*, 175–205, doi:10.1016/0040-1951(80)90234-6.

Sleep, N. H. (1997), Application of a unified rate and state friction theory to the mechanics of fault zones with strain localization, *J. Geophys. Res.*, *102*(B2), 2875–2895, doi:10.1029/96JB03410.

Sleep, N. H. (2006), Frictional dilatancy, *Geochem. Geophys. Geosyst.*, *7*, Q10008, doi:10.1029/2006GC001374.

Stein, R. S. (1999), The role of stress transfer in earthquake occurrence, *Nature*, *402*, 605–609, doi:10.1038/45144.

Swan, G. (1983), Determination of stiffness and other joint properties from roughness measurements, *Rock Mech. Rock. Eng.*, *16*, 19–38.

Walsh, J. B., and M. A. Grosenbaugh (1979), A new model for analyzing the effect of fractures on compressibility, *J. Geophys. Res.*, *84*, 3532–3536, doi:10.1029/JB084iB07p03532.

Wesnousky, S. G. (2006), Predicting the endpoints of earthquake ruptures, *Nature*, *444*, 358–360.

Yoshioka, N. (1994), Elastic behavior of contacting surfaces under normal loads: A computer simulation using three-dimensional surface topographies, *J. Geophys. Res.*, *99*, 15,549–15,560, doi:10.1029/94JB00938.

Yoshioka, N., and K. Iwasa (2006), A laboratory experiment to monitor the contact state of a fault by transmission waves, *Tectonophysics*, *413*, 221–238, doi:10.1016/j.tecto.2005.10.035.